




# Dietary advanced glycation end-products exacerbate sarcopenia onset by activating apoptosis through PRMT1-mediated CRT3 arginine methylation

Tian-Jin Huang<sup>1,2</sup> · Shu Shang<sup>1,2</sup> · Qin Wan<sup>1,2</sup> · Qiang Li<sup>1,2</sup> · Yang-Jingsi Li<sup>1,2</sup> · Jin-Na Zheng<sup>3</sup> · Fa-Xiu Chen<sup>1,2</sup> 

Received: 19 October 2024 / Revised: 10 March 2025 / Accepted: 11 March 2025  
© The Author(s) 2025

## Abstract

**Background** Sarcopenia, the age-related decline in muscle mass and function, poses a major health risk to the elderly population. Although dietary advanced glycation end-products (AGEs) have been implicated in worsening sarcopenia, the precise molecular mechanisms remain unclear.

**Methods** A sarcopenia animal model was established by feeding a high AGE diet to C57BL/6 mice. Muscle function and mass were assessed using grip strength tests, and rotarod tests. Proteomic analysis was used to identify differentially expressed proteins. Immunoprecipitation, mass spectrometry, and co-immunoprecipitation were employed to investigate protein interactions both in vivo and in vitro. Quantitative reverse transcription PCR and Western blotting were conducted to measure gene and protein expression levels.

**Results** Our results revealed that dietary AGEs accelerated the onset of sarcopenia in mice by triggering apoptosis. Proteomic analysis showed a marked upregulation of protein arginine methyltransferase 1 (PRMT1) in the muscle tissues of mice fed a high AGE diet. PRMT1 mediated the arginine methylation of CREB-regulated transcription coactivator 3 (CRT3) at the R534 site within its transactivation domain, leading to CRT3 activation. The activated CRT3, together with Forkhead box O3a (FOXO3a), transactivated the *BAX* (BCL2 associated X) gene, initiating Bax downstream signaling, promoting apoptosis in muscle cells, and contributing to muscle atrophy. Inhibition of PRMT1 prevented CRT3 methylation and suppressed Bax-mediated apoptotic signaling in vitro. Moreover, in vivo treatment with PRMT1 and Bax inhibitors significantly attenuated AGE-induced sarcopenia in mice.

**Conclusion** PRMT1-mediated CRT3 arginine methylation plays a critical role in AGE-induced sarcopenia and suggests potential therapeutic targets for preventing sarcopenia progression.

**Keywords** Sarcopenia · PRMT1 · CRT3 · FOXO3a · Bax · Apoptosis · Arginine methylation

## Introduction

Sarcopenia, characterized by the progressive loss of skeletal muscle mass and function, is a growing health concern among the aging population [1, 2]. This condition not only impairs mobility and quality of life but also increases the risk of falls, fractures, and mortality in the elderly [1, 2]. Clinically, the management of sarcopenia primarily focuses on resistance exercise and nutritional interventions, including protein supplementation and vitamin D, aimed at improving muscle strength and mass [3–5]. Pharmacological treatments are still in the early stages, with agents like myostatin inhibitors and selective androgen receptor modulators (SARMs) being investigated for their potential to

✉ Fa-Xiu Chen  
fa-xiu.chen@hotmail.com

<sup>1</sup> Department of Geriatrics, Jiangxi Provincial People's Hospital, No. 92 Aiguo Rd, Donghu District, Nanchang, Jiangxi 330006, China  
<sup>2</sup> Department of Geriatrics, The First Affiliated Hospital of Nanchang Medical College, No. 92 Aiguo Rd, Donghu District, Nanchang, Jiangxi 330006, China  
<sup>3</sup> Medical College of Nanchang University, Nanchang, Jiangxi 330006, China

enhance muscle growth and function [6–8]. However, these approaches have shown limited efficacy, and the underlying molecular mechanisms driving sarcopenia remain incompletely understood, underscoring the need for novel therapeutic strategies.

Among the various factors contributing to sarcopenia, dietary influences have garnered increasing attention due to their potential to modulate the progression of the disease [3–5]. Advanced glycation end-products (AGEs) are a diverse group of compounds formed through the non-enzymatic glycation of proteins, lipids, and nucleic acids [9–11]. AGEs can be categorized into free and protein-bound forms, with notable examples including N $\epsilon$ -carboxymethyl-lysine (CML), N $\epsilon$ -1-carboxyethyl-lysine (CEL), and N $\delta$ -(5-hydroxy-5-methyl-4-imidazolone-2-yl)-ornithine (MG-H1) [9–11]. These compounds accumulate naturally in the body with age and are also ingested through AGE-rich foods, particularly those subjected to high-temperature cooking methods such as grilling, frying, and baking [9–11]. AGEs interact with the receptor for advanced glycation end-products (RAGE), a multi-ligand receptor that triggers a cascade of intracellular signaling pathways, including the activation of nuclear factor-kappa B (NF- $\kappa$ B), mitogen-activated protein kinases (MAPKs), and the Janus kinase/signal transducers and activators of transcription (JAK/STAT) pathway [9–11]. These signaling events lead to increased oxidative stress, inflammation, and cellular apoptosis, all of which contribute to the progression of sarcopenia [9–11]. However, the precise molecular mechanisms by which AGEs influence muscle degeneration remain largely unknown.

Protein arginine methylation is a post-translational modification that regulates various cellular processes, including gene expression, signal transduction, and protein-protein interactions [12–14]. The protein arginine methyltransferase (PRMT) family consists of nine members, classified into three types based on the type of methylation they catalyze [12–14]. Type I PRMTs, including PRMT1, PRMT2, PRMT3, PRMT4, PRMT6, and PRMT8, catalyze asymmetric dimethylation of arginine (ADMA) residues [12–14]. PRMT1, the predominant PRMT, is responsible for the majority of cellular arginine methylation and plays crucial roles in transcriptional regulation and signal transduction [12–14]. PRMT4 is primarily involved in the regulation of gene expression by modifying histones, while PRMT6 is known for its role in DNA repair and chromatin organization [12–14]. Type II PRMTs, including PRMT5 and PRMT9, catalyze symmetric dimethylation of arginine (SDMA) and are involved in processes such as RNA splicing and the regulation of myelination [12–14]. PRMT5 is particularly important in the regulation of gene silencing and the maintenance of stem cell pluripotency [12–14]. Type III PRMT, which includes PRMT7, catalyzes monomethylation of arginine

residues and has been implicated in cellular differentiation and response to stress [12–14]. Beyond their essential roles in normal cellular functions, PRMTs have gained increasing recognition for their involvement in the development of various diseases. Dysregulation of PRMTs has been implicated in the pathogenesis of cancer, cardiovascular diseases, neurodegenerative disorders, and immune system dysfunctions [12–14]. Recent studies reveal that the PRMT family also plays a critical role in regulating skeletal muscle atrophy through pathways involving autophagy, protein degradation, and muscle stem cell regeneration [15, 16]. PRMT1 is central to this process, acting via the PRMT6–FOXO3 (Forkhead box O3) axis and AMPK–PGC-1 $\alpha$  (AMP-activated protein kinase–Peroxisome proliferator-activated receptor-gamma coactivator 1 alpha) signaling during muscle remodeling [15, 16]. Additionally, PRMT7 modulates PGC-1 $\alpha$  expression through interactions with p38 and ATF2 (Activating transcription factor 2), while CARM1 (Coactivator-associated arginine methyltransferase 1) enhances autophagic responses under glucose deprivation by stabilizing itself through the AMPK–SKP2–CARM1 pathway [17, 18].

Apoptosis, or programmed cell death, plays a pivotal role in the maintenance of tissue homeostasis and is tightly regulated by a complex network of signaling pathways [19, 20]. The BCL-2 (B-cell leukemia/lymphoma 2) family of proteins, which includes both pro-apoptotic and anti-apoptotic members, is central to the regulation of mitochondrial-mediated apoptosis [19, 20]. Bax (BCL2-associated X protein) is a key pro-apoptotic member that promotes apoptosis by permeabilizing the mitochondrial outer membrane, leading to the release of cytochrome c and the activation of caspases, which are the executioners of apoptosis [19, 20]. Upstream regulators of Bax include various transcription factors such as p53 and FOXO3a, which can induce *BAX* expression in response to cellular stress signals [19, 20]. Downstream, Bax-mediated apoptosis is amplified through the mitochondrial pathway, culminating in the activation of caspase-3, which drives the execution phase of apoptosis [19, 20]. Apoptosis has been increasingly recognized as a critical mechanism contributing to muscle loss [21–24]. Enhanced Bax expression and activity have been observed in aging muscle, correlating with increased muscle cell apoptosis and atrophy [21–24]. The chronic activation of apoptotic pathways in muscle cells leads to the progressive depletion of myocytes, thereby exacerbating the decline in muscle mass and function characteristic of sarcopenia [21–24]. However, the underlying mechanism driving Bax overexpression in the pathogenesis of sarcopenia remains elusive.

In this study, we aimed to investigate dysregulated proteins in AGE-induced sarcopenia and identify key proteins and their associated signaling pathways involved in

the condition. Through proteomic analysis, we found that PRMT1 was significantly upregulated in AGE-induced muscle. Further analysis identified CREB-regulated transcription coactivator 3 (CRTC3) as a critical substrate of PRMT1 in muscle cells. Our findings suggested that PRMT1-mediated methylation of CRTC3 at the R534 site activated CRTC3, which, in cooperation with FOXO3a, transactivated the *BAX* gene, leading to apoptosis and muscle degradation. Additionally, we demonstrated that inhibiting PRMT1 effectively reversed these effects, underscoring the therapeutic potential of targeting this pathway to combat sarcopenia.

## Materials and methods

### Animal experiments

C57BL/6J mice were obtained from Beijing Vital River Laboratory Animal Technology Co. (Beijing, China) and were housed under specific-pathogen-free (SPF) conditions at a temperature of 22 °C, with a 12-hour light-dark cycle. To induce sarcopenia, eight-week-old C57BL/6J mice (weighing approximately 22–25 g) were randomly assigned to a control group and an experimental group ( $n=8$  per group). The experimental group was fed a diet enriched with high levels of AGEs, referred to as HAGE, for 24 weeks, while the control group received a standard diet with low AGEs (LAGE) (Zeigler; #AIN-93G). The HAGE diet was prepared by heating the LAGE diet at 160 °C for 30 min as described previously [25]. Body weight was monitored weekly throughout the study. After the 24-week dietary intervention, 32-week-old mice were evaluated for signs of sarcopenia, including grip strength test, rotarod test, and determination of muscle mass/body weight ratio. The mice were then humanely euthanized via carbon dioxide (CO<sub>2</sub>) inhalation followed by cervical dislocation to ensure death.

To assess the effectiveness of the inhibitors, eight-week-old C57BL/6J mice (approximately 22–25 g) were randomly assigned to five groups ( $n=8$  per group). One group was maintained on a LAGE diet, while the other four groups were fed an HAGE diet. Within the HAGE diet groups, one subset received intraperitoneal injections of phosphate-buffered saline (PBS) as a control, while the other subsets were treated with specific inhibitors: PPMT1 inhibitor (TCE5003) (MedChemExpress; #HY-107574; 50 mg/kg), type I PRMT inhibitor (MS023) (MedChemExpress; #HY-19615; 50 mg/kg), and Bax inhibitor (BAI1) (MedChemExpress; #HY-103269; 50 mg/kg). The inhibitors were administered weekly over a 24-week period. All animal experiments were conducted in accordance with the

guidelines of the Institutional Animal Care and Use Committee (IACUC) of Jiangxi Provincial People's Hospital.

### Measurement of non-fasting blood glucose and haemoglobin A1c (HbA1c) levels

Mice were anesthetized weekly with 3% isoflurane (Sigma-Aldrich, #792632) at a consistent time period (3:00–4:00 PM) to minimize stress associated with sample collection. A small blood sample (about 50 µL) was obtained from the tail vein using a sterile lancet. For non-fasting blood glucose measurement, approximately 3 µL of blood was analyzed immediately using a glucometer (Roche Diagnostics; #Accu-Chek). For HbA1c measurement, 10 µL of whole blood was processed using an HbA1c assay kit (Crystal Chem; #80310) according to the manufacturer's instructions.

### Grip strength test

The grip strength of the mice was assessed using a grip strength meter following a previous protocol [26]. Each mouse was gently held by the tail base and positioned over the grid of the meter, allowing them to grasp the grid with both forelimbs. The mouse was then gently pulled back in a horizontal position until it released its grip. The maximum force exerted at the point of release was recorded. This process was repeated five times for each mouse, with a one-minute interval between each trial to avoid fatigue.

### Rotarod test

The motor coordination and balance of the mice were evaluated using a Rotarod apparatus (Ugo Basile; #47650) according to a previous method [26]. Mice were placed on a rotating rod with a diameter of 3 cm, which accelerated from 4 to 40 revolutions per minute (rpm) over a 300-second period. The time taken for each mouse to fall from the rotating rod was recorded. Each mouse underwent three consecutive trials, with one-minute intervals between trials to minimize fatigue. The average time to fall across the three trials was calculated and used as the measure of motor performance.

### Determination of bilateral gastrocnemius muscle mass relative to body weight

Upon euthanasia, the mid-belly region of the gastrocnemius (GAS) muscles was dissected from each mouse, cleaned of connective tissue and fat, and weighed using an analytical balance. The combined mass of the left and right gastrocnemius muscles was calculated. To account for differences in

body size, the total muscle mass was expressed as a percentage of the mouse's body weight.

### Skeletal muscle isolation

Skeletal muscle tissue was isolated from HAGE-induced sarcopenia model mice and age-matched control mice. Mice were euthanized using CO<sub>2</sub> asphyxiation, followed by cervical dislocation to ensure complete euthanasia. The gastrocnemius and soleus muscles were carefully dissected from both hind limbs, quickly rinsed in ice-cold PBS, blotted dry, and immediately snap-frozen in liquid nitrogen. The frozen muscle tissues were stored at -80 °C until further processing.

### Hematoxylin and eosin (H&E) staining

Skeletal muscle tissues from sarcopenia model mice were first fixed in 4% paraformaldehyde (Sigma-Aldrich; #158127) overnight at 4 °C. After fixation, the tissues were dehydrated through a graded series of ethanol solutions, cleared in xylene (Sigma-Aldrich; #534056), and embedded in paraffin (Leica Biosystems; #39601006). Paraffin-embedded tissues were then sectioned at 5 µm thickness using a microtome (Leica Biosystems; #RM2235). The tissue sections were deparaffinized in xylene and rehydrated through a graded series of ethanol to distilled water. Sections were stained with hematoxylin (Sigma-Aldrich; #H9627) for 5 min, rinsed in running tap water, and then differentiated in 1% acid alcohol. After rinsing again, sections were stained with eosin Y solution (Thermo Fisher; #6766007) for 2 min, followed by dehydration in graded ethanol, clearing in xylene, and mounting with a coverslip using a mounting medium (Thermo Fisher; #9990402). The stained sections were then visualized under a light microscope (Olympus; #BX53) for histological analysis. The cross-sectional area (CSA) was measured and analyzed using ImageJ software (National Institutes of Health, USA; #version 2018) following previously described methods [27, 28].

### Cell culture and transfection

C2C12 myoblasts were obtained from American Type Culture Collection (ATCC; #CRL-1772) and cultured in Dulbecco's Modified Eagle Medium (DMEM) (Gibco; #11965092) supplemented with 10% fetal bovine serum (FBS; Gibco; #26140079) and 1% penicillin-streptomycin (Gibco; #15140122) at 37 °C in a humidified atmosphere containing 5% CO<sub>2</sub>. Cells were seeded in 6-well plates and allowed to reach approximately 70–80% confluence before transfection. For the generation of stable cell lines, C2C12 cells were transfected with shRNAs (2 µg per 10<sup>7</sup> cells) (Table S1) or plasmids (4 µg of DNA per 10<sup>7</sup> cells) (Table

S2) using Lipofectamine 3000 (Invitrogen; #L3000015) according to the manufacturer's instructions. After 48 h of transfection, cells were selected with 2 µg/mL puromycin (Sigma-Aldrich; #P8833) for 10 days for shRNA transfection or 600 µg/mL G418 (Sigma-Aldrich; #A1720) for 14 days for plasmid transfection. Selection was continued until non-transfected control cells were completely eliminated. The resulting stable cell lines were maintained in selection media to ensure the persistence of gene expression.

### Isobaric tag for relative and absolute quantitation (iTRAQ) analysis

The iTRAQ proteomics analysis was performed following a previous protocol [29]. For analysis in muscle, tissues ( $n=3$  per group, tissues of equal weight pooled within each group) were homogenized in lysis buffer (7 M urea, 2 M thiourea, 4% CHAPS, 40 mM Tris, pH 8.5, and 1 mM PMSF) using a Dounce homogenizer on ice. For iTRAQ assay in cells, Control<sup>OE</sup> and PRMT1<sup>OE</sup> cells ( $n=3$  wells per cell line, pooled before protein extraction) were harvested by trypsinization, washed with PBS, and lysed in RIPA buffer (Thermo Fisher; #89900) containing a protease inhibitor cocktail (Thermo Fisher; #78429). The homogenates from muscle tissues and cell lysates were centrifuged at 15,000 ×  $g$  for 20 min at 4 °C to remove insoluble debris. Protein concentration was determined using the Bradford assay (Thermo Fisher; #A55866). An equal amount of protein (100 µg) from each sample was reduced, alkylated, and digested with trypsin (Thermo Fisher; #90057) overnight at 37 °C. The resulting peptides were labeled with iTRAQ reagents (Sigma-Aldrich; #4352135) according to the manufacturer's instructions. Labeled peptides were pooled and subjected to strong cation exchange (SCX) chromatography using an SCX column (Thermo Fisher; #074643) followed by high-performance liquid chromatography (HPLC) separation. The fractions were analyzed by liquid chromatography-tandem mass spectrometry (LC-MS/MS) using a Q Exactive mass spectrometer (Thermo Fisher; #0726090).

Data analysis was performed using the Proteome Discoverer software (Thermo Fisher), with peptide and protein identification conducted against the UniProt Mus musculus database. Trypsin was designated as the cleavage enzyme, permitting up to 4 missed cleavages. The precursor ion mass tolerance was set to 20 ppm during the first search and refined to 5 ppm for the main search, while the fragment ion mass tolerance was maintained at 0.02 Da. The false discovery rate (FDR) was controlled below 0.01, and the minimum score threshold for modified peptides was set to greater than 40. Gene Ontology (GO) analysis (<http://www.geneontology.org>) was conducted to classify the differentially expressed proteins (DEPs) into functional categories,

including molecular functions, biological processes, and cellular components.

### Western blot

Skeletal muscle tissues were isolated from sarcopenia model mice and age-matched control mice, then homogenized in ice-cold radioimmunoprecipitation assay (RIPA) buffer (Thermo Fisher; #89900) with a protease inhibitor cocktail. Cultured cells were similarly lysed. The homogenates and cell lysates were incubated on ice for 30 min and centrifuged at  $15,000 \times g$  for 20 min at 4 °C, with supernatants collected for protein quantification using the BCA assay. Equal amounts of protein (40 µg) from each sample were mixed with 4 × Laemmli sample buffer (Bio-Rad; #1610747) and boiled for 5 min at 95 °C. The samples were then loaded onto 10–12% SDS-PAGE gels and separated by electrophoresis. After electrophoresis, the proteins were transferred onto PVDF membranes (Millipore; #IPVH00010) using a wet transfer system (Bio-Rad; #1703930). Following transfer, the membranes were blocked in 5% non-fat dry milk (Bio-Rad; #1706404) in Tris-buffered saline with 0.1% Tween-20 (TBST) for 1 h at room temperature. The membranes were then incubated overnight at 4 °C with primary antibodies diluted in 5% BSA (Sigma-Aldrich; #A9647) in TBST. The specific primary antibodies used for the detection of target proteins were listed in Table S3. After washing, membranes were treated with HRP-conjugated secondary antibodies (Table S3), visualized with ECL substrate (Thermo Fisher; #32106).

### Assessment of PRMT1 activity Inhibition by TCE5003 and MS023

The inhibitory effects of TCE5003 and MS023 on PRMT1 activity were evaluated using the PRMT1 Chemiluminescent Assay Kit (BPS Bioscience, #52004L) according to the methods provided by the manufacturer. This assay relied on the detection of methylation at the R3 residue of Histone H4 using a highly specific antibody. Recombinant mouse PRMT1 protein (Abcam, #ab78937) was used in place of the human PRMT1 enzyme provided in the kit. Briefly, the assay was initiated by incubating S-adenosylmethionine (SAM) with mouse PRMT1 (3 µg), assay buffer, and varying concentrations of the inhibitors TCE5003 (0, 1.5, 3, and 4.5 µM) or MS023 (0, 30, 60, and 90 nM). After the enzymatic reaction, a primary antibody specific to the methylated R3 residue of Histone H4 (BPS Bioscience, #52150) was added to detect methyltransferase activity. Subsequently, an HRP-labeled secondary antibody (BPS Bioscience, #52131H) was applied to amplify the signal. The chemiluminescence signal generated was measured using

a microplate luminometer (BioTek), with signal intensity directly reflecting the activity of PRMT1.

To evaluate the effects of TCE5003 and MS023 on PRMT1 protein levels, C2C12 cells were treated with varying concentrations of TCE5003 (0, 1.5, 3, and 4.5 µM) or MS023 (0, 30, 60, and 90 nM) for 12 h. Following treatment, PRMT1 protein levels were assessed via Western blot analysis.

### Immunoprecipitation (IP) and mass spectrometry analysis

For immunoprecipitation, muscle tissue and cultured cell lysates were centrifuged at  $16,000 \times g$  for 10 min at 4 °C. The supernatants were then pre-cleared by incubation with protein G beads (Thermo Fisher; #20397) for 1 h at 4 °C. Following pre-clearance, 5 µg of primary antibody or isotype-matched IgG control (Table S3) was added to the lysates, which were then incubated overnight at 4 °C. To capture the immune complexes, protein G beads were introduced to the lysates and allowed to incubate for 3 h at 4 °C. The beads were subsequently washed three times with a wash buffer composed of 100 mM NaCl, 50 mM Tris (pH 7.5), 0.1% NP-40, 3% glycerol, and 100 mM phenylmethylsulfonyl fluoride (PMSF). The bound proteins were eluted by adding 2 × Laemmli sample buffer, followed by heating at 95 °C for 5 min. The eluted proteins were then subjected to Western blot analysis. For mass spectrometry, the visualized protein bands on the SDS-PAGE gels were cut into nearly 1 mm small slices and digested with trypsin. The eluted peptides were analyzed using liquid LC-MS/MS. The resulting data were processed using Proteome Discoverer software to identify and quantify the proteins present in the samples.

### Co-immunoprecipitation (Co-IP)

C2C12 cells were transfected with pCDNA3-Flag-CRTC3 + pCDNA3-MYC-FOXO3a and pCDNA3-Flag-CRTC3<sup>R534K</sup> + pCDNA3-MYC-FOXO3a plasmids using Lipofectamine 3000 following the manufacturer's protocol. After 48 h of transfection, the cells were treated with 100 µM AGE-BSA (Sigma-Aldrich; #121800) in combination with either 3.0 µM TCE5003 or 90 nM MS023 for 12 h. Subsequently, the cells were lysed in ice-cold RIPA buffer containing a protease inhibitor cocktail, and the lysates were clarified by centrifugation at  $16,000 \times g$  for 10 min at 4 °C. The supernatants were subjected to immunoprecipitation by incubating with anti-Flag beads (Thermo Fisher; #A36797) or anti-MYC beads (Thermo Fisher; #20168) overnight at 4 °C. After washing three times with a buffer containing 100 mM NaCl, 50 mM Tris (pH 7.5), 0.1% NP-40, and

3% glycerol, the bound proteins were eluted by heating the beads in  $2 \times$  Laemmli sample buffer at 95 °C for 5 min. The eluted proteins were separated by SDS-PAGE and protein interactions were determined by western blots.

### RNA isolation and quantitative reverse transcription polymerase chain reaction (RT-qPCR)

Total RNA was extracted from cells using the TRIzol reagent (Thermo Fisher; #15596026) according to the manufacturer's instructions. Briefly, cells were lysed directly in TRIzol reagent, and the lysates were homogenized by pipetting. Chloroform (Sigma-Aldrich; #C2432) was added to the lysates, and the mixture was centrifuged at  $12,000 \times g$  for 15 min at 4 °C to separate the aqueous phase. The RNA was precipitated from the aqueous phase by adding isopropanol (Sigma-Aldrich; #I9516), followed by centrifugation at  $12,000 \times g$  for 10 min at 4 °C. The RNA pellet was washed with 75% ethanol, air-dried, and resuspended in RNase-free water. For RT-qPCR, 1 µg of total RNA was reverse transcribed using the PrimeScript RT reagent Kit (Takara; #RR037A) following the manufacturer's protocol. RT-qPCR was performed using the TB Green Premix Ex Taq II (Takara; #RR820A). The expression levels of target genes were normalized to  $\beta$ -actin as an internal control. The relative expression of genes was calculated using the  $2^{-\Delta\Delta Ct}$  method. Primers used for RT-qPCR were listed in Table S4.

### Chromatin Immunoprecipitation (ChIP) assay

Three independent experiments were conducted as follows: (1) Control<sup>KD</sup> and CRT3<sup>KD</sup> cells were treated with 100 µM AGE-BSA for 12 h; (2) C2C12 cells were treated with different concentrations of AGE-BSA (0, 25, 50, and 100 µM) for 12 h; (3) C2C12 cells were co-treated with 100 µM AGE-BSA in combination with varying doses of TCE5003 (0, 1.5, and 3 µM) or MS023 (0, 30, and 60 nM) for 12 h. Following treatment, all cells were cross-linked with 1% formaldehyde (Sigma-Aldrich; #252549) for 10 min at room temperature to fix protein-DNA interactions. Cross-linking was quenched by adding glycine to a final concentration of 125 mM. The cells were then washed with ice-cold PBS and lysed in ChIP lysis buffer (Santa Cruz Biotechnology; #sc-45000) containing protease inhibitors. The lysates were sonicated to shear the chromatin into 200–500 bp fragments. The chromatin was immunoprecipitated using anti-CRT3 and anti-FOXO3a antibodies (Table S3) with Protein G beads overnight at 4 °C. The immune complexes were washed sequentially with ChIP wash buffer (Santa Cruz Biotechnology; #sc-45002) and then eluted in ChIP elution buffer (Santa Cruz Biotechnology; #sc-45003). Cross-links were reversed by incubating the samples at 65 °C overnight,

followed by treatment with RNase A (Thermo Fisher; #EN0531) and proteinase K (Thermo Fisher; #EO0491). The DNA was purified using a PCR purification kit (Qiagen; #28106) and analyzed by qPCR using primers specific to gene promoters (Table S5) to assess the binding of CRT3 and FOXO3a.

### In vitro methylation assays

For in vitro methylation assays, His-CRT3 proteins were purified from BL-21 *E. coli* cells. The pET28a-CRT3 vector was introduced into BL-21 *E. coli*, and protein expression was induced by adding 100 µM IPTG (isopropyl  $\beta$ -D-1-thiogalactopyranoside; Sigma-Aldrich; #I6758) at 16 °C for 12 h. After induction, the bacteria were lysed in a lysis buffer (50 mM Tris, 150 mM NaCl, 10 mM Imidazole, 1 mM PMSF, 0.1% NP-40, 2 mM MgCl<sub>2</sub>, and 1 mM DTT) through sonication for 15 min. The lysates were centrifuged at  $10,000 \times g$  for 30 min at 4 °C to remove cellular debris. The His-CRT3 proteins in the supernatant were purified by incubating with Ni-NTA agarose (Thermo Fisher; #R90115) for 3 h, followed by washing four times with wash buffer (50 mM Tris-HCl, pH 7.4, 300 mM NaCl, 40 mM Imidazole, 1 mM PMSF, and 0.1% NP-40). For the methylation reaction, 10 µg of purified His-CRT3 proteins were incubated with 1 mM S-(5'-Adenosyl)-L-methionine chloride (SAM) (Sigma-Aldrich; #539209) as a methyl donor, in the presence or absence of 1 µg of PRMT1 protein (Abcam; #ab78937) and either 3 µM TCE5003 or 90 nM MS023 as inhibitors. The reaction mixture was incubated at 30 °C for 1.5 h. After incubation, the reaction products were then analyzed by SDS-PAGE to assess methylation status.

### Quantification of ages in plasma and muscle skeletal tissues

The quantification of AGEs was conducted using LC-MS/MS based on a previously established protocol [30]. Plasma samples were prepared by mixing 50 µL of plasma with an equal volume of sodium phosphate buffer (Sigma-Aldrich; #DB0222) containing protease inhibitors (Sigma-Aldrich; #S8820). The mixture was briefly vortexed and centrifuged at  $12,000 \times g$  for 15 min at 4 °C. The supernatant was collected and stored at -80 °C until further analysis. For muscle tissues, approximately 100 mg of tissue was homogenized in 100 µL of ice-cold sodium phosphate buffer supplemented with protease inhibitors, followed by centrifugation at  $12,000 \times g$  for 20 min at 4 °C. The resulting supernatants were used for subsequent analyses. Chromatographic separation was performed on a reverse-phase C18 column (Acquity UPLC BEH C18, 50  $\times$  2.1 mm, 1.7 µm; Waters Corporation; #186002350) with a gradient elution system.

The mobile phases consisted of 5 mmol/L ammonia solution (Phase A) and acetonitrile (Phase B), and the column temperature was maintained at 48 °C. The gradient elution began with 98% Phase A and 2% Phase B, gradually transitioning to 60% Phase A and 40% Phase B over 10 min, followed by re-equilibration to initial conditions. The flow rate was set to 800  $\mu$ L/min, with an injection volume of 2  $\mu$ L. Quantification of CML, CEL, and MG-H1 was performed by comparing the peak area ratios of analytes to their corresponding stable isotope-labeled internal standards. Calibration curves were established using standard solutions at known concentrations. The electrospray ionization source was operated in positive ion mode with the following parameters: capillary voltage of 0.5 kV, source temperature of 150 °C, desolvation temperature of 600 °C, desolvation gas flow at 800 L/h, and cone gas flow at 50 L/h. Data acquisition and analysis were carried out using MassLynx software (V4.1, SCN 644, Waters). Quantitative data were processed by integrating the peak areas using the TargetLynx module.

### Flow cytometry (FACS) analysis

Cells were harvested and washed twice with cold PBS, then resuspended in  $1\times$  Annexin V binding buffer (BD Biosciences; #556454) at a concentration of  $1\times 10^6$  cells/mL. Subsequently, 5  $\mu$ L of Annexin V-FITC (BD Biosciences; #556419) and 5  $\mu$ L of Propidium Iodide (PI) (BD Biosciences; #556463) were added to 100  $\mu$ L of the cell suspension. The mixture was incubated in the dark at room temperature for 10 min. After incubation, 400  $\mu$ L of Annexin V binding buffer was added to each sample, and the stained cells were analyzed immediately using a flow cytometer (BD FACSCanto II). Data were acquired and analyzed using FlowJo software to quantify the proportions of living cells (Quadrant 1), necrotic cells (Quadrant 2), late apoptotic cells (Quadrant 3), and early apoptotic cells (Quadrant 4). All experiments were performed in triplicate to ensure reproducibility.

### Statistical analyses

Statistical analyses were performed using SPSS (Statistical Package for the Social Sciences; IBM, version 22) software. Data were presented as mean  $\pm$  standard deviation (SD). Comparisons between two groups were made using unpaired Student's *t*-tests. For multiple group comparisons, one-way ANOVA followed by Tukey's post-hoc test was used to determine statistical significance. *P*-values less than 0.05 were considered statistically significant. All experiments were conducted with at least three biological replicates to ensure reproducibility.

## Results

### HAGE diet exacerbated sarcopenia incidence in mice

Several clinical studies have statistically shown a positive correlation between a HAGE diet or AGE accumulation in the body and the onset of sarcopenia [31–34]. To investigate the relationship and specific molecular mechanisms between a HAGE diet and the development of sarcopenia, we fed 8-week-old C57BL/6 mice with either a LAGE diet or a HAGE diet, dividing them into two groups. After 24 weeks, we assessed whether sarcopenia had developed in the mice (Fig. 1A). We monitored non-fasting blood glucose and HbA1c levels weekly over the 24-week period. The results showed that non-fasting blood glucose and HbA1c levels were significantly higher in the HAGE group compared to the LAGE group (Fig. 1B and C). Additionally, we measured the levels of free and protein-bound AGEs in the serum and skeletal muscle tissues. The results indicated that levels of free and protein-bound CML and CEL, as well as free MG-H1, were elevated in the HAGE group compared to the LAGE group (Fig. 1D and I and S1). However, the levels of protein-bound MG-H1 in serum and muscle tissues from HAGE mice were similar to those in LAGE mice (Fig. 1I and S1).

To evaluate the incidence of sarcopenia, we measured several relevant parameters. The HAGE group exhibited poorer motor function, as evidenced by reduced grip strength (HAGE:  $48.3\pm 5.2$  gm  $\times$  Force, LAGE:  $71.3\pm 8.5$  gm  $\times$  Force,  $P<0.01$ ) (Fig. 1J) and shorter latency to fall in rotarod tests (HAGE:  $10.3\pm 1.7$  s, LAGE:  $22.5\pm 2.3$  s,  $P<0.01$ ) (Fig. 1K). Furthermore, the skeletal muscle mass index was significantly lower in the HAGE group compared to the LAGE group (HAGE:  $0.48\pm 0.05\%$ , LAGE:  $1.16\pm 0.12\%$ ,  $P<0.001$ ) (Fig. 1L). Histological analysis of skeletal muscle tissues revealed significant muscle damage in the HAGE group, characterized by a reduction in muscle fiber size and an increase in connective tissue (Fig. 1M). Quantification of CSA of muscle fibers revealed a significant reduction in the HAGE group (Fig. 1N). These physiological and pathological indicators suggested that feeding mice a HAGE diet induced the development of sarcopenia.

### PRMT1 and key molecules of the intrinsic apoptotic pathway were significantly elevated in HAGE-induced sarcopenic mice

To identify the key molecules involved in HAGE-induced sarcopenia, we isolated skeletal muscle from mice, extracted the proteins, digested them with trypsin, and labeled them using the iTRAQ method. Mass spectrometry analysis was then performed to identify differentially expressed proteins

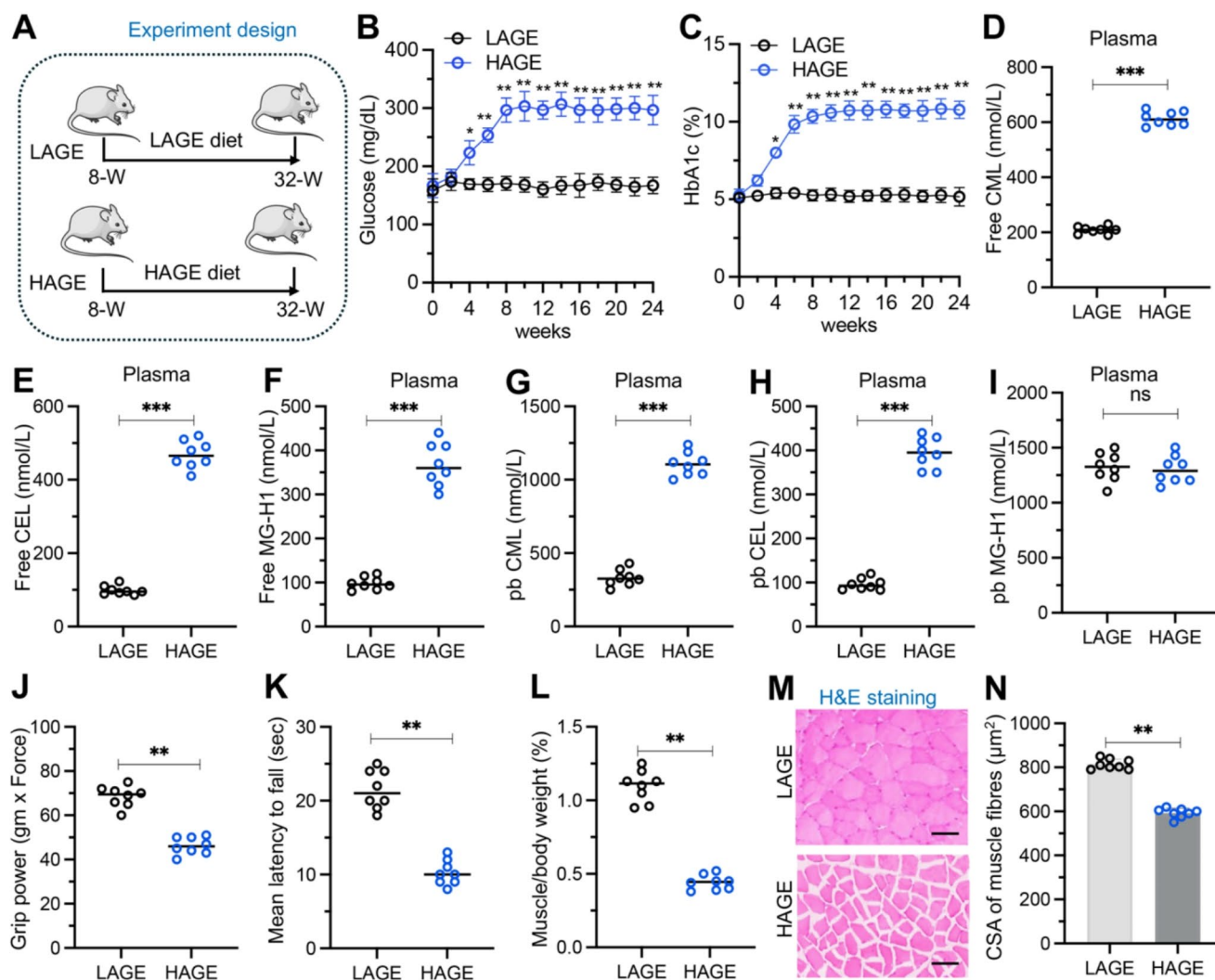


**Fig. 1** Feeding a HAGE diet increased the incidence of sarcopenia in mice (**A**) Experimental design. (**B**) Non-fasting blood glucose levels in mice fed LAGE and HAGE diets ( $n=8$  per group) at different time points. (**C**) HbA1c levels in mice fed LAGE and HAGE diets ( $n=8$  per group) at different time points. (**D-I**) Concentrations of free and protein-bound (pb) CML, CEL, and MG-H1 in plasma from mice fed LAGE and HAGE diets ( $n=8$  per group). (**D**) Free CML in plasma.

(**E**) Free CEL in plasma. (**F**) Free MG-H1 in plasma. (**G**) pb-CML in plasma. (**H**) pb-CEL in plasma. (**I**) pb-MG-H1 in plasma. (**J**) Grip strength. (**K**) Latency to fall as assessed by the rotarod test. (**L**) Muscle-to-body weight ratio. (**M**) Representative images of skeletal muscle stained with H&E. Bars=100  $\mu$ m. (**N**) Quantified CSA of muscle fibers ( $\mu$ m<sup>2</sup>) ( $n=8$  per group). ns: no significant difference; \* $P<0.05$ ; \*\* $P<0.01$ ; \*\*\* $P<0.001$

(Fig. 2A). In skeletal muscle from HAGE-fed mice, we identified 317 DEPs (Table S6), including 198 upregulated and 119 downregulated proteins (Table S6). Figure 2B showed the top 15 most significantly upregulated and downregulated proteins. Among the upregulated proteins, PRMT1 showed the most significant increase, along with a notable upregulation of the receptor for AGEs, RAGE. Additionally, key proteins in the intrinsic apoptotic pathway, such as Bax, Apaf1 (Apoptotic protease activating factor-1), Caspase 3 (Casp3), Caspase 7 (Casp7), and Caspase 9 (Casp9), were significantly elevated (Fig. 2B). Other proteins with marked upregulation included CRTC3, FTO (Fat mass and obesity-associated), MMP2/7/9 (Matrix metalloproteinase 2, 7, and

9), and ADAMTS2/6 (A disintegrin and metalloproteinase with thrombospondin motifs 2 and 6) (Fig. 2B). The five most significantly downregulated proteins were USP2 (Ubiquitin specific peptidase 2), YTHDF3 (YTH N6-methyladenosine RNA binding protein 3), LMOD1 (Leiomodin 1), SLPI (Secretory leukocyte peptidase inhibitor), and LBP (Lipopolysaccharide binding protein) (Fig. 2B). GO analysis of the DEPs revealed that the upregulated proteins were primarily involved in biological processes such as apoptotic signaling pathways, extracellular matrix disassembly, organic acid catabolic processes, cellular response to oxidative stress, glucose transport, and DNA damage response (Fig. 2C). In contrast, the downregulated proteins were

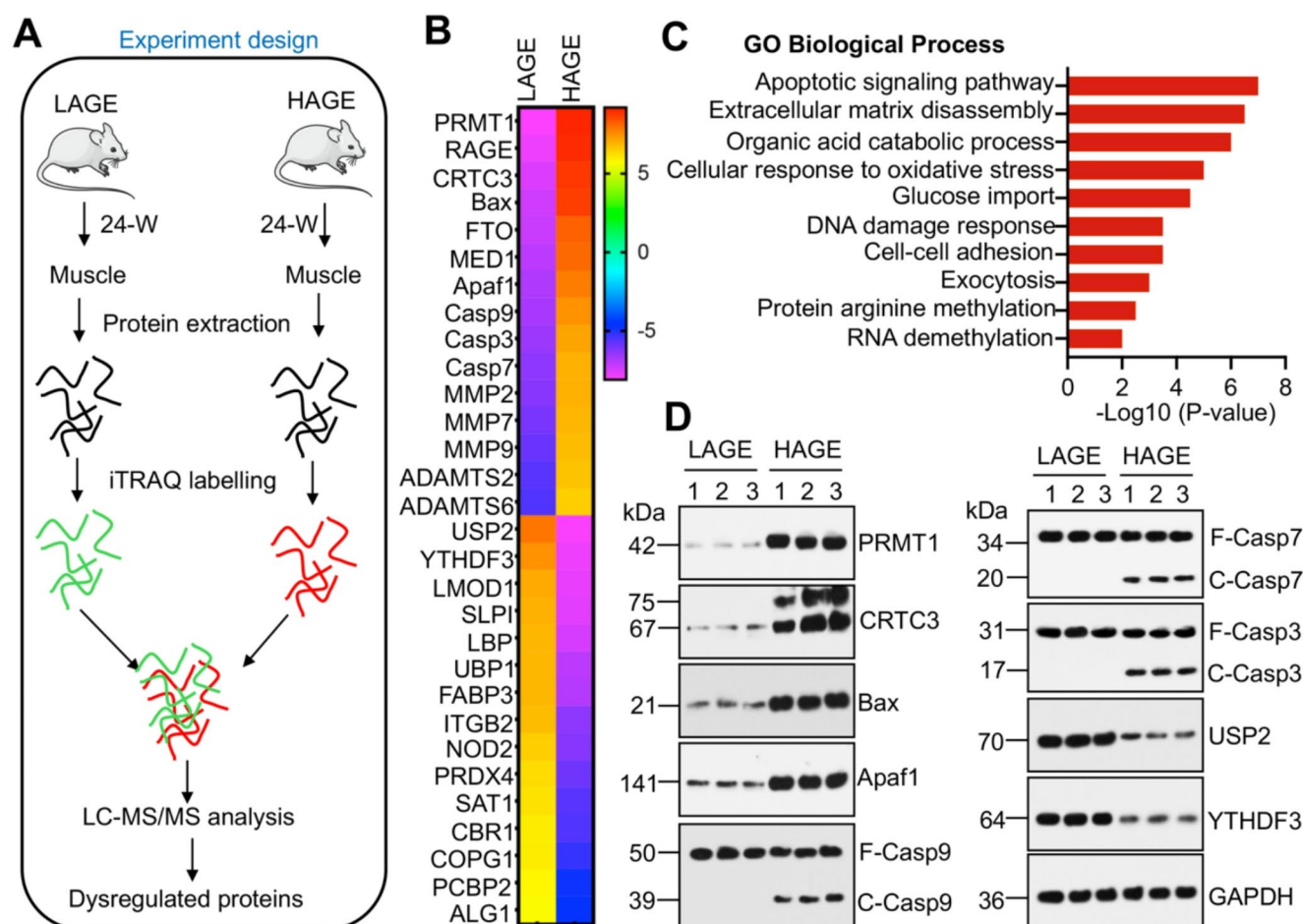


**Fig. 2** PRMT1, CRTC3, and apoptotic molecules were upregulated in sarcopenic muscle tissues. **(A)** Experimental design for iTRAQ analysis. **(B)** The top 15 upregulated and top 15 downregulated proteins in skeletal muscle tissues from the LAGE and HAGE groups of mice. **(C)** Gene Ontology (GO) analysis of biological processes associated with

the upregulated proteins. **(D)** Validation of protein levels for PRMT1, CRTC3, Bax, Apaf1, Casp3, Casp7, Casp9, USP2, and YTHDF3 in skeletal muscle tissues from the LAGE and HAGE groups of mice ( $n=3$  per group) using Western blotting

mainly associated with muscle tissue development, protein catabolic processes, energy metabolism, regulation of gene expression, and oxidative phosphorylation (Fig. S2).

To validate the accuracy of the mass spectrometry results, we examined the expression of several representative proteins, including PRMT1, CRTC3, Bax, Apaf1, Casp3, Casp7, Casp9, USP2, and YTHDF3, in skeletal muscle tissues from both LAGE and HAGE mice ( $n=3$  per group). The results confirmed that the expression patterns of all tested proteins were consistent with the iTRAQ quantification data (Fig. 2D).

### PRMT1 and key molecules of the intrinsic apoptotic pathway were significantly elevated in AGE-BSA-treated myoblast cells

To determine whether the altered protein expression observed in Fig. 2D was directly regulated by AGEs, we

treated C2C12 cells in vitro with different concentrations of AGE-BSA (0, 25, 50, and 100  $\mu$ M) for 12 h and then assessed the expression levels of PRMT1, CRTC3, Bax, Apaf1, Casp3, Casp7, Casp9, USP2, and YTHDF3. The results showed that the expression of PRMT1, CRTC3, Bax, Apaf1, Casp3, Casp7, and Casp9 increased in a dose-dependent manner with higher concentrations of AGE-BSA, whereas the expression of USP2 and YTHDF3 gradually decreased with increasing AGE-BSA doses (Fig. S3). These in vitro findings suggested that PRMT1 and key molecules of the intrinsic apoptotic pathway were directly regulated by AGEs.

### Inhibition of PRMT1 in HAGE-fed mice prevented sarcopenia incidence

Given the critical role of PRMTs in the development of various diseases [12–14] and the significant upregulation of

PRMT1 in the muscle tissues of HAGE-induced sarcopenic mice, we aimed to explore the involvement of PRMT1 in the development of sarcopenia. To investigate whether inhibiting PRMT1 could prevent sarcopenia, we selected TCE5003, a specific PRMT1 inhibitor, and MS023, a type I PRMT inhibitor. In vitro studies confirmed that both inhibitors selectively reduced PRMT1 activity without altering its protein levels (Fig. S4A–S4E).

For in vivo analysis, mice were divided into four groups: LAGE diet, HAGE diet, HAGE diet with weekly TCE5003 injections, and HAGE diet with weekly MS023 injections, over a 24-week period (Fig. 3A). Throughout this period, non-fasting blood glucose and HbA1c levels in the TCE5003- and MS023-treated groups were comparable to those in the HAGE group and significantly higher than those in the LAGE group (Fig. 3B and C). Additionally, the levels of free and protein-bound CML and CEL, as well as free MG-H1, were elevated in the serum and skeletal muscle tissues of the TCE5003-treated, MS023-treated, and HAGE groups compared to the LAGE group (Fig. 3D and I and S5). However, protein-bound MG-H1 levels showed no significant differences among the groups (Fig. 3I and S5). These results indicated that TCE5003 and MS023 treatments did not impact the accumulation of AGEs in the serum and muscle tissues. Remarkably, treatment with TCE5003 and MS023 significantly mitigated the development of sarcopenia in HAGE-fed mice. Specifically, both inhibitors partially restored grip strength (TCE5003:  $58.9 \pm 4.8$  gm  $\times$  Force; MS023:  $59.7 \pm 6.5$  gm  $\times$  Force; HAGE:  $47.3 \pm 3.9$  gm  $\times$  Force; LAGE:  $72.4 \pm 6.8$  gm  $\times$  Force) (Fig. 3J), latency to fall (TCE5003:  $17.4 \pm 1.5$  s; MS023:  $18.2 \pm 2.2$  s; HAGE:  $10.3 \pm 1.0$  s; LAGE:  $24.6 \pm 2.1$  s) (Fig. 3K), and skeletal muscle mass index (TCE5003:  $0.84 \pm 0.07\%$ ; MS023:  $0.81 \pm 0.04\%$ ; HAGE:  $0.55 \pm 0.04\%$ ; LAGE:  $1.17 \pm 0.23\%$ ) (Fig. 3L). Histological analysis of skeletal muscle tissues revealed that TCE5003 and MS023 treatment significantly increased muscle fiber size and reduced connective tissue accumulation compared to the HAGE group (Fig. 3M). Quantification of CSA of muscle fibers in TCE5003 and MS023 groups was significantly increased compared to the HAGE group, although these values remained lower than those observed in the LAGE group (Fig. 3N).

As PRMT1 functions as a protein arginine methyltransferase, we assessed arginine methylation levels in total cell extracts derived from the muscle tissues of mice in the LAGE, HAGE, TCE5003, and MS023 groups. The results demonstrated significantly elevated levels of ADMA in the HAGE group compared to the other three groups (Fig. S6). While ADMA levels in the TCE5003 and MS023 groups were similar to those observed in the LAGE group (Fig. S6).

## Protein levels of CRTC3 and key molecules of the intrinsic apoptotic pathway were dependent on PRMT1

To investigate the target proteins of PRMT1, we transfected C2C12 cells with pCDNA3-empty vector and pCDNA3-PRMT1 plasmids to establish two independent Control<sup>OE</sup> and PRMT1<sup>OE</sup> cell lines (Fig. S7). Using these cell lines, we performed iTRAQ-based quantitative proteomics and mass spectrometry analysis to identify DEPs regulated by PRMT1 (Fig. 4A). The mass spectrometry results revealed that overexpression of PRMT1 led to differential expression of 206 proteins, with 135 proteins being upregulated and 71 proteins downregulated (Table S7). Figure 4B highlighted the top 10 most upregulated and top 10 most downregulated proteins. Interestingly, among the upregulated proteins, we identified CRTC3, Bax, Apaf1, Casp3, Casp7, and Casp9 (Fig. 4B). We further confirmed the expression levels of CRTC3, Bax, Apaf1, Casp3, Casp7, and Casp9 in two Control<sup>OE</sup> and two PRMT1<sup>OE</sup> cell lines, observing that CRTC3, Bax, and Apaf1 were upregulated, while Casp3, Casp7, and Casp9 were activated in PRMT1<sup>OE</sup> cells (Fig. 4C). These findings suggest that overexpression of PRMT1 can lead to the activation of the intrinsic apoptotic pathway. To further validate this, we conducted Annexin V-FITC/PI staining in Control<sup>OE1</sup> and PRMT1<sup>OE1</sup> cell lines. The results showed a significant increase in the distribution of cells in the Q3 (late apoptotic cells) and Q4 (early apoptotic cells) quadrants in PRMT1<sup>OE1</sup> cells compared to Control<sup>OE1</sup> cells (2.16% vs. 80.2%) (Fig. 4D). These results indicate that overexpression of PRMT1 induces intrinsic apoptosis in C2C12 cells.

We established Control<sup>KD</sup> and PRMT1<sup>KD</sup> cell lines in C2C12 cells (Fig. S8A and S8B) and treated them with or without 100  $\mu$ M AGE-BSA for 12 h. Protein levels of PRMT1, CRTC3, Bax, Apaf1, Casp3, Casp7, and Casp9 were subsequently analyzed. The results showed that PRMT1 depletion failed to increase the protein levels of CRTC3, Bax, Apaf1, Casp3, Casp7, and Casp9 (Fig. S8C). These findings suggested that PRMT1 knockdown did not induce intrinsic apoptosis in AGE-BSA-treated C2C12 cells.

## PRMT1 methylated CRTC3 in vivo and in vitro

Since PRMT1 is an arginine methyltransferase and both CRTC3 and downstream apoptotic molecules of Bax were dependent on PRMT1, we speculated that PRMT1 may mediate the arginine methylation of these molecules. To test this hypothesis, we conducted IP experiments in skeletal muscle from HAGE-fed mice using IgG and PRMT1 antibodies. We found that PRMT1 bound only to CRTC3 and not to Bax or its downstream apoptotic molecules (Fig. 5A),

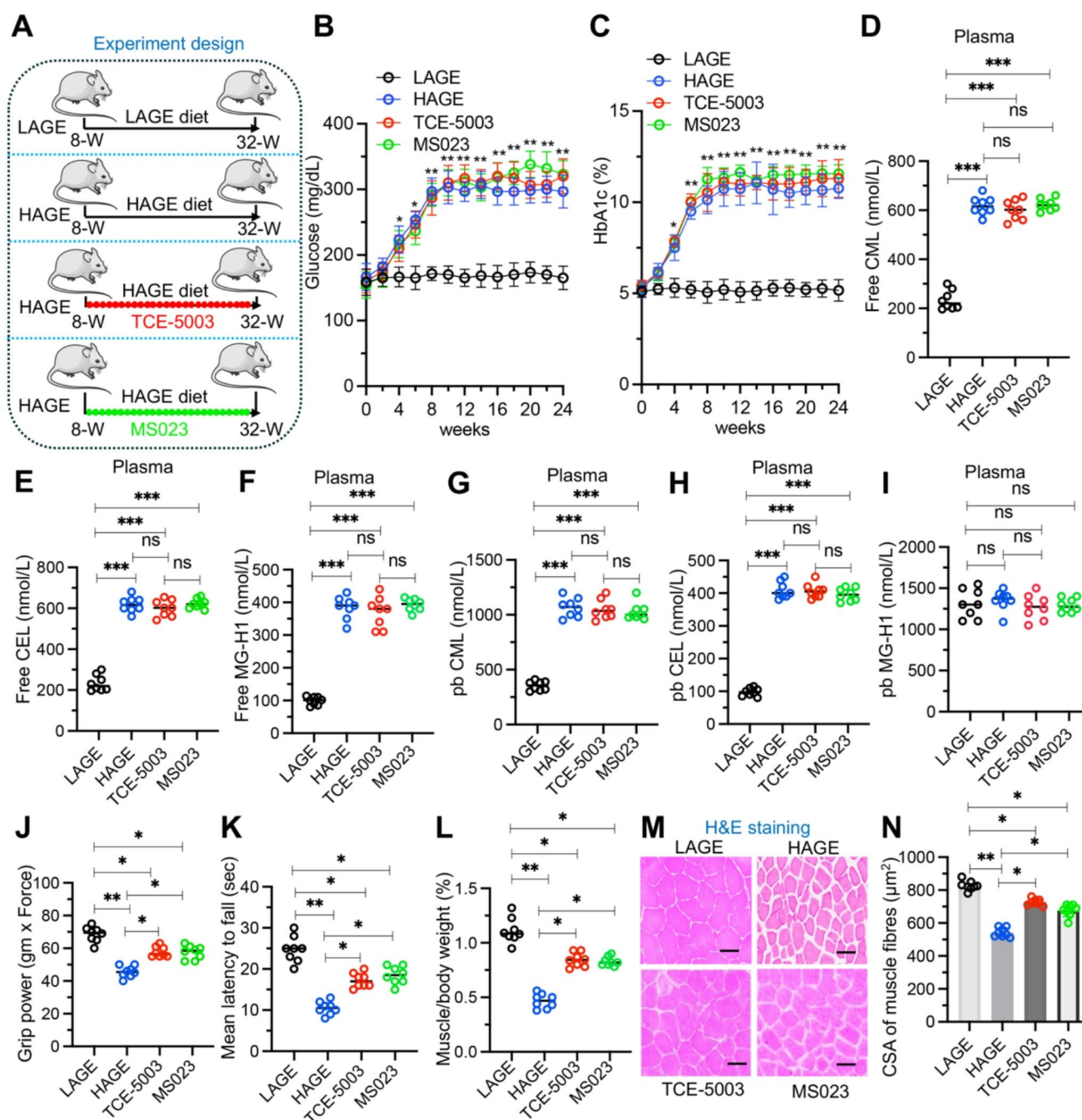


**Fig. 3** Administration of TCE5003 and MS023 partially prevented the development of sarcopenia in HAGE-fed mice. **(A)** Experimental design of TCE5003 and MS023 injections. **(B)** Non-fasting blood glucose levels in LAGE, HAGE, HAGE+TCE5003, and HAGE+MS023 groups of mice ( $n=8$  per group) at different time points. **(C)** HbA1c levels in LAGE, HAGE, HAGE+TCE5003, and HAGE+MS023 groups of mice ( $n=8$  per group) at different time points. **(D–I)** Concentrations of free and pb CML, CEL, and MG-H1 in plasma from LAGE,

HAGE, HAGE+TCE5003, and HAGE+MS023 groups of mice ( $n=8$  per group). **(D)** Free CML in plasma. **(E)** Free CEL in plasma. **(F)** Free MG-H1 in plasma. **(G)** pb-CML in plasma. **(H)** pb-CEL in plasma. **(I)** pb-MG-H1 in plasma. **(J)** Grip strength. **(K)** Latency to fall as assessed by the rotarod test. **(L)** Muscle-to-body weight ratio. **(M)** Representative images of skeletal muscle stained with H&E. Bars = 100  $\mu\text{m}$ . **(N)** Quantified CSA of muscle fibers ( $\mu\text{m}^2$ ) ( $n=8$  per group). ns: no significant difference; \* $P<0.05$ ; \*\* $P<0.01$ ; \*\*\* $P<0.001$

suggesting that PRMT1 might be involved in the arginine methylation of CRTC3. Next, we co-transfected HA-CRTC3 and various Flag-tagged PRMTs (PRMT1/2/3/4/5) into C2C12 cells and performed IP with anti-HA agarose.

Our results showed that CRTC3 bound exclusively to PRMT1 and not to the other PRMTs (Fig. 5B). Additionally, anti-ADMA detection revealed that only PRMT1 could trigger ADMA modification of CRTC3 (Fig. 5B). Furthermore,

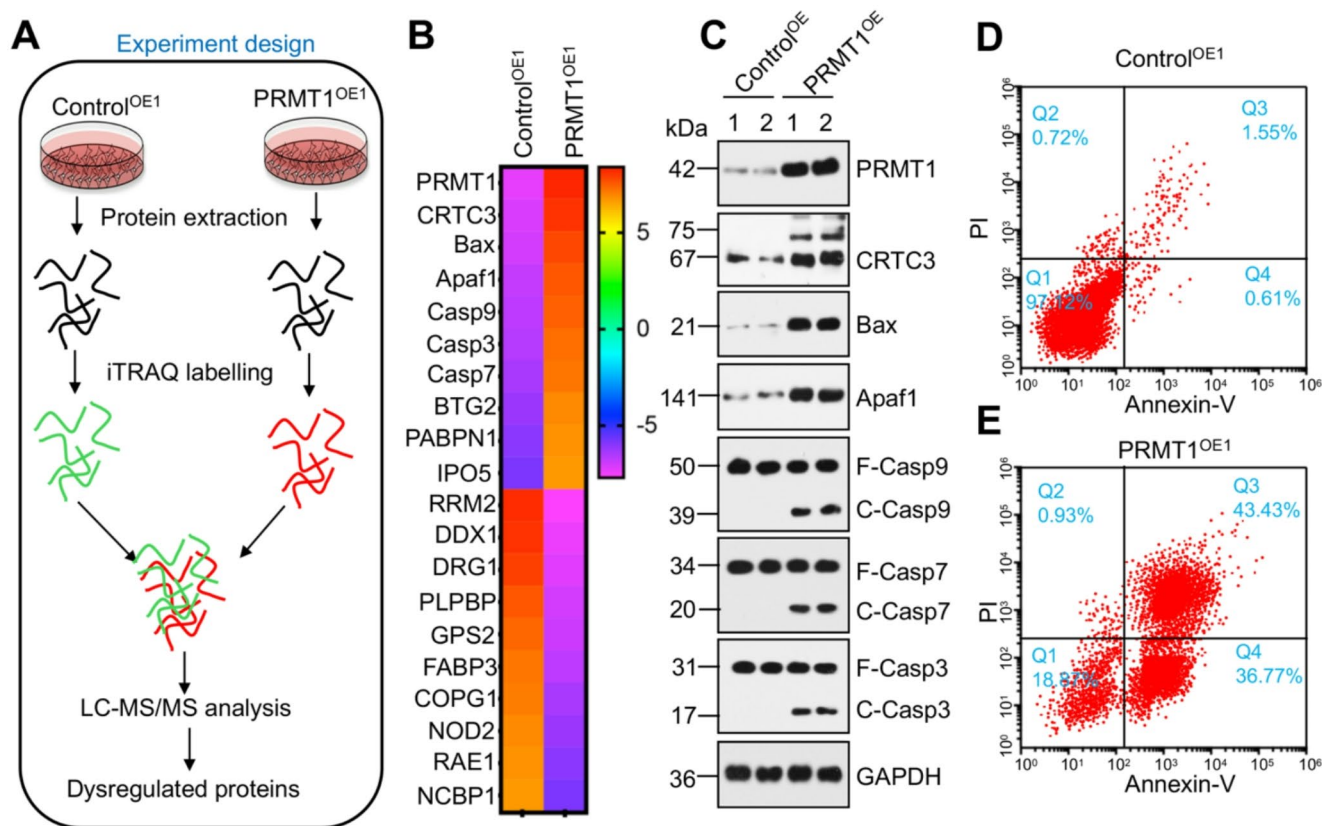


**Fig. 4** CRTC3 and apoptotic molecules were dependent on PRMT1. **(A)** Experimental design for iTRAQ analysis. **(B)** The top 10 upregulated and top 10 downregulated proteins in Control<sup>OE1</sup> and PRMT1<sup>OE1</sup> cells. **(C)** Validation of protein levels for PRMT1, CRTC3, Bax, Apaf1, Casp3, Casp7, and Casp9 in two independent Control<sup>OE</sup> and PRMT1<sup>OE</sup>

cell lines using Western blotting. **(D and E)** Flow cytometry analysis. Control<sup>OE1</sup> **(D)** and PRMT1<sup>OE1</sup> **(E)** cells were stained with Annexin V-FITC and Propidium Iodide (PI) for 10 min at room temperature in the dark. Stained cells were analyzed using a fluorescence-activated cell sorter. The percentage of cells in different quadrants was indicated

we co-transfected C2C12 cells with HA-CRTC3 and Flag-tagged PRMT1 constructs containing the catalytic-dead mutants (G98R, E162Q, and E171A). We found that these PRMT1 mutants were unable to bind or methylate CRTC3 (Fig. 5C). In an in vitro methylation assay using recombinant PRMT1 and His-CRTC3, PRMT1 successfully methylated CRTC3 (Fig. 5D). The addition of TCE5003 and MS023 completely inhibited the methylation of CRTC3 in this assay (Fig. 5D).

To identify the specific arginine methylation site(s) on CRTC3, we divided CRTC3 into three regions [R1 (1–150 aa), R2 (151–525 aa), and R3 (526–619 aa)] (Fig. 5E and S9). The in vitro methylation assay revealed that PRMT1 only methylated the R3 region (Fig. 5F). Within the R3 region, there were three arginine residues: R534, R615, and R618 (Fig. S9). We mutated these three residues to lysine and found that PRMT1 could not methylate the R534K mutant (Fig. 5G), indicating that R534 was the specific site of PRMT1-mediated arginine methylation on CRTC3.

### CRTC3 and FOXO3a synergistically regulated the expression of the BAX gene

Since CRTC3 is a transcriptional coactivator [35], we hypothesized that it might be involved in regulating Bax and its downstream apoptotic molecules. To test this hypothesis, we generated Control<sup>KD1</sup>, Control<sup>KD2</sup>, CRTC3<sup>KD1</sup>, and CRTC3<sup>KD2</sup> cell lines in C2C12 background (Fig. S10A). After treating the cells with 100  $\mu$ M AGE-BSA, we measured the expression levels of *BAX*, *APAF1*, *CASP3*, *CASP7*, and *CASP9*. We found that knockdown of CRTC3 specifically reduced the expression of *BAX*, while the expression of *APAF1*, *CASP3*, *CASP7*, and *CASP9* remained unaffected (Fig. S10A). We also performed ChIP assays to examine whether CRTC3 could bind to the promoter regions of these genes. The results showed that CRTC3 was specifically enriched at the *BAX* gene promoter (Fig. S10B–S10F).

As a transcriptional co-regulator, CRTC3 required interaction with transcription factors to regulate gene expression. To identify the transcription factors interacting with CRTC3, we conducted IP with anti-CRTC3 in skeletal

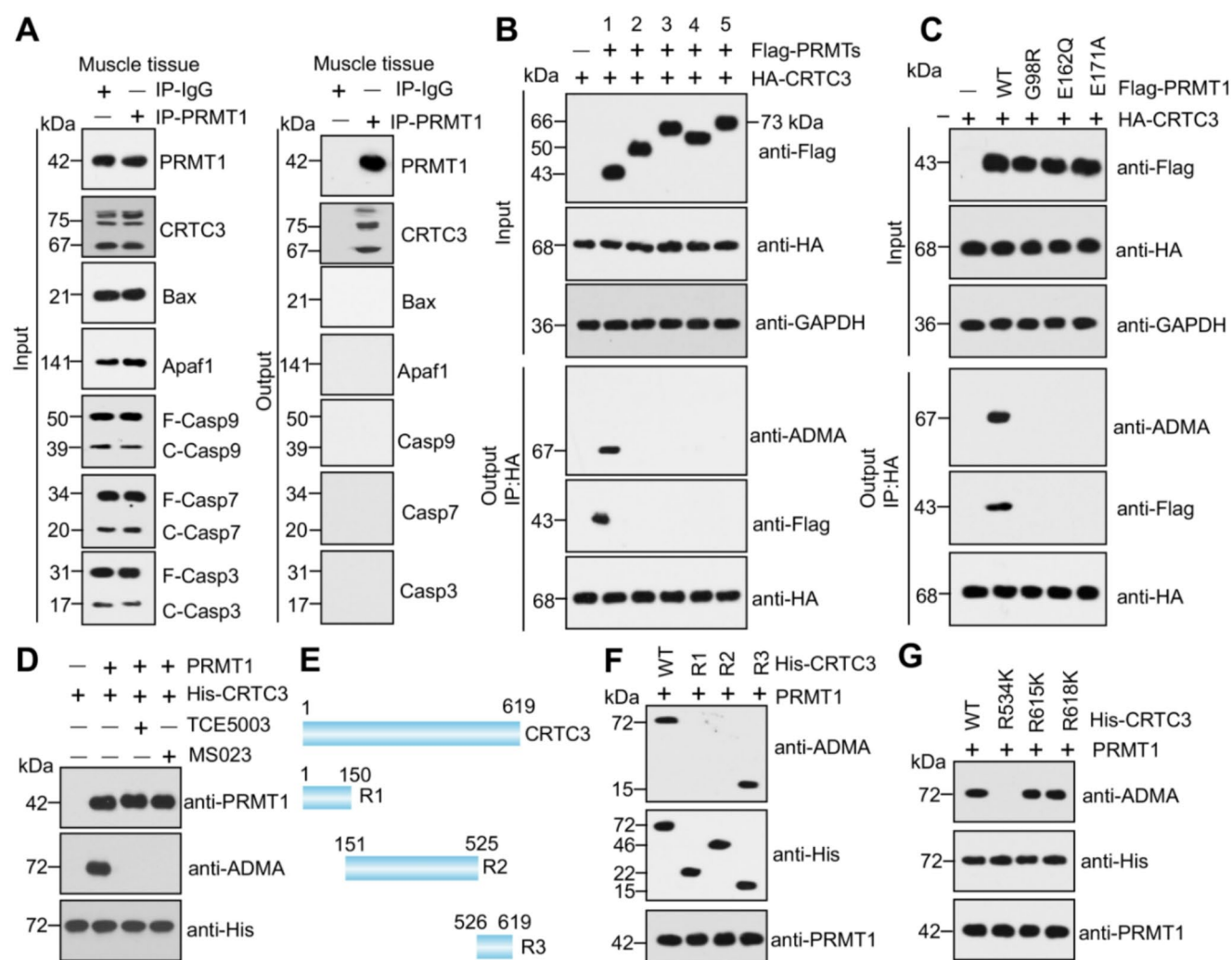


**Fig. 5** PRMT1 interacted with the methylated CRTC3 in vivo and in vitro. **(A)** PRMT1 interacted with CRTC3 in vivo. Protein extracts from skeletal muscle tissues were immunoprecipitated using IgG and anti-PRMT1-conjugated protein G. Input and immunoprecipitated samples were probed for PRMT1, CRTC3, Bax, Apaf1, Casp3, Casp7, and Casp9. **(B)** PRMT1 interacted with CRTC3 in vitro. C2C12 cells were co-transfected with Flag-tagged PRMTs (1/2/3/4/5) and HA-tagged CRTC3. After 48 h, cells were lysed and immunoprecipitated using anti-HA agarose. Input and immunoprecipitated samples were analyzed using anti-Flag, anti-HA, anti-ADMA, and GAPDH antibodies. **(C)** PRMT1 methylated CRTC3 in an enzyme activity-dependent manner. C2C12 cells were co-transfected with HA-CRTC3 and Flag-tagged PRMT1 constructs containing catalytic-dead mutants (G98R, E162Q, and E171A). After 48 h, cells were lysed and immunoprecipitated using anti-HA agarose. Input and immunoprecipitated samples

were analyzed using anti-Flag, anti-HA, anti-ADMA, and GAPDH antibodies. **(D)** TCE5003 and MS023 disrupted the interaction and methylation of CRTC3 by PRMT1 in vitro. An in vitro methylation assay was conducted using recombinant PRMT1 and His-tagged CRTC3, both in the presence and absence of TCE5003 (3.0  $\mu$ M) and MS023 (90 nM). Immunoblots were performed using anti-ADMA, anti-His, and anti-PRMT1 antibodies. **(E)** Different regions of the CRTC3 protein: R1 (1–150 aa), R2 (151–525 aa), and R3 (526–619 aa). **(F)** PRMT1 interacted with the R3 region of CRTC3 in vitro. **(G)** PRMT1 methylated the R534 site of CRTC3. An in vitro methylation assay was performed using recombinant PRMT1 and His-tagged CRTC3 or its mutants (CRTC3<sup>R534K</sup>, CRTC3<sup>R615K</sup>, or CRTC3<sup>R618K</sup>). Immunoblots were performed using anti-ADMA, anti-His, and anti-PRMT1 antibodies

muscle tissues from HAGE-fed mice, followed by mass spectrometry analysis. This analysis identified 82 proteins that interact with CRTC3 (Table S8), among which only one transcription factor, FOXO3a, was detected (Table S8). Using the same IP products utilized for mass spectrometry analysis, we confirmed that CRTC3 interacted with FOXO3a (Fig. 6A). Additionally, an IP assay performed

on the same skeletal muscle tissues using an anti-FOXO3a antibody validated that FOXO3a could reciprocally pull down CRTC3 (Fig. 6B). In C2C12 cells co-transfected with Flag-CRTC3 and MYC-FOXO3a, no interaction between CRTC3 and FOXO3a was observed in the absence of AGE-BSA treatment. However, following AGE-BSA treatment, CRTC3 and FOXO3a formed a direct interaction (Fig. 6C).

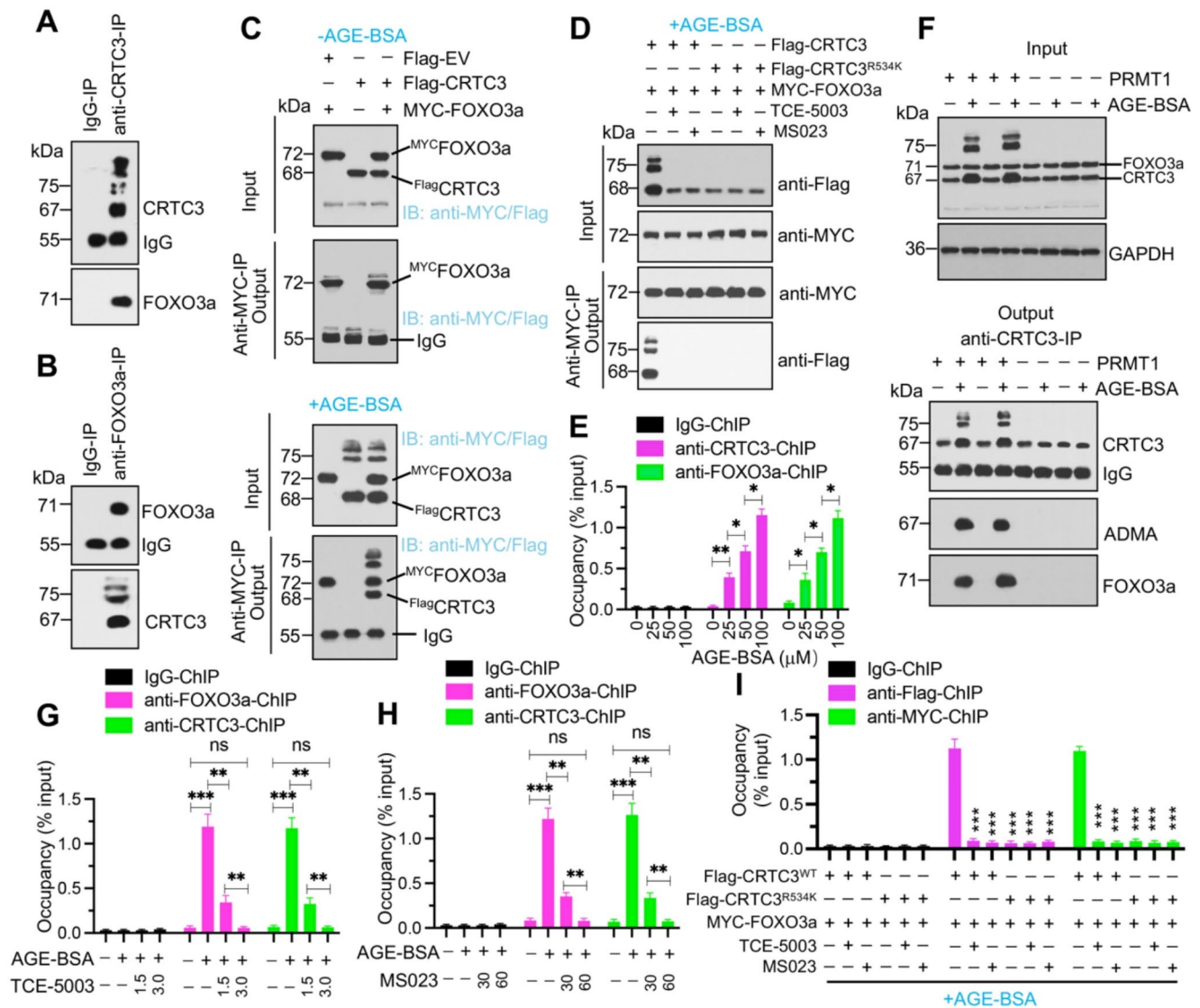


**Fig. 6** CRTC3 interacted with FOXO3a to regulate the expression of *BAX*. **(A)** CRTC3 immunoprecipitated with FOXO3a in vivo. Skeletal muscle tissues from HAGE-fed mice were immunoprecipitated using IgG or anti-CRTC3, followed by Western blot with anti-CRTC3 and anti-FOXO3a. **(B)** FOXO3a immunoprecipitated with CRTC3 in vivo. Skeletal muscle tissues from HAGE-fed mice were immunoprecipitated using IgG or anti-FOXO3a, followed by Western blot with anti-CRTC3 and anti-FOXO3a. **(C)** CRTC3 interacted with FOXO3a in vitro. C2C12 cells were co-transfected with Flag-tagged and MYC-tagged plasmids, treated with or without AGE-BSA, and analyzed by immunoprecipitation and Western blot. Membranes were simultaneously probed using anti-Flag and anti-MYC. **(D)** TCE5003 and MS023 inhibited the CRTC3-FOXO3a interaction in vitro. Co-IP assays were performed on cells co-expressing Flag-CRTC3+MYC-FOXO3 and Flag-CRTC3<sup>R534K</sup>+MYC-FOXO3. The cells were treated with 100  $\mu$ M AGE-BSA combined with either 3.0  $\mu$ M TCE5003 or 90 nM MS023 for 12 h. **(E)** The occupancy of CRTC3 and FOXO3a on the *BAX* promoter was dose-dependent on AGE-BSA. C2C12 cells were treated with increasing concentrations (0, 25, 50, and 100  $\mu$ M)

of AGE-BSA for 12 h, followed by ChIP and RT-qPCR to assess promoter occupancy. **(F)** Knockdown of PRMT1 disrupted the interaction between CRTC3 and FOXO3a. Two independent PRMT1<sup>KD</sup> cell lines were treated with or without 100  $\mu$ M AGE-BSA for 12 h. IP assays were performed using anti-CRTC3-conjugated protein A agarose, and the purified proteins were analyzed by Western blot using anti-CRTC3, anti-FOXO3a, and anti-ADMA antibodies. The membranes loading input samples were simultaneously probed with anti-Flag and anti-MYC antibodies. **(G and H)** TCE5003 and MS023 reduced the occupancy of FOXO3a and CRTC3 on the *BAX* promoter in a dose-dependent manner. C2C12 cells were treated with 100  $\mu$ M AGE-BSA and increasing concentrations of TCE5003 (0, 1.5, and 3  $\mu$ M) **(G)** or MS023 (0, 30, and 60 nM) **(H)** for 12 h. ChIP followed by RT-qPCR was performed to quantify the binding of CRTC3 and FOXO3a to the *BAX* promoter. **(I)** CRTC3<sup>R534K</sup> failed to bind to the *BAX* promoter. Cells, as used in (D), were subjected to ChIP assays with anti-Flag and anti-MYC antibodies, followed by RT-qPCR to assess the binding of CRTC3, CRTC3<sup>R534K</sup>, and FOXO3a to the *BAX* promoter. ns: no significant difference. \*\* $P < 0.01$

Interestingly, the CRTC3<sup>R534K</sup> mutant failed to interact with FOXO3a even under AGE-BSA treatment (Fig. 6D). Furthermore, the PRMT1 inhibitors TCE5003 and MS023 disrupted the interaction between CRTC3 and FOXO3a in AGE-BSA-treated cells (Fig. 6D).

We also examined the effects of AGE-BSA on the expression of *BAX* gene and found AGE-BSA treatment significantly induced the expression of the *BAX* gene (Fig. S11A and S11B). However, co-treatment with TCE5003 or MS023 alongside AGE-BSA reduced *BAX* expression in a dose-dependent manner as the concentrations of TCE5003 and MS023 increased (Fig. S11A and S11B). ChIP assays conducted on C2C12 cells treated with varying concentrations of AGE-BSA (0, 25, 50, and 100  $\mu$ M) revealed enrichment of both FOXO3a and CRTC3 at the *BAX* gene promoter (Fig. 6E). Using the same PRMT1<sup>KD</sup> cells in Fig. S8C, IP assays were performed using an anti-CRTC3 antibody and the results demonstrated that CRTC3 could not interact with FOXO3a even under 100  $\mu$ M AGE-BSA treatment (Fig. 6F). Furthermore, the methylation levels of CRTC3 were completely abolished in PRMT1<sup>KD</sup> cells treated with AGE-BSA (Fig. 6F). To further evaluate the impact of PRMT1 inhibition on promoter binding, C2C12 cells were co-treated with 100  $\mu$ M AGE-BSA and increasing concentrations of either TCE5003 (0, 1.5, and 3  $\mu$ M) or MS023 (0, 30, and 60 nM). ChIP assays revealed a dose-dependent decrease in the occupancy of CRTC3 and FOXO3a on the *BAX* promoter with both TCE5003 and MS023 treatments (Fig. 6G and H). Using the cells depicted in Fig. 6D, we measured *BAX* mRNA levels and observed that the CRTC3<sup>R534K</sup> mutant failed to induce *BAX* expression following AGE-BSA treatment (Fig. S11C). Furthermore, ChIP assays using anti-Flag and anti-MYC antibodies in these cells demonstrated that CRTC3<sup>R534K</sup> did not bind to the promoter region of the *BAX* gene under AGE-BSA treatment conditions (Fig. 6I). Collectively, these results indicated that PRMT1-mediated methylation was critical for the interaction between CRTC3 and FOXO3a. Inhibition of PRMT1 by TCE5003 or MS023 reduced the binding of CRTC3 and FOXO3a to the *BAX* gene promoter, potentially mitigating *BAX* gene expression and its downstream apoptotic effects.

### Inhibition of Bax blocked AGE-BSA-induced apoptosis in vitro and prevented sarcopenia incidence in HAGE-fed mice

Given that Bax and its downstream apoptotic signaling pathways were activated in both HAGE-fed mice and AGE-BSA-treated C2C12 cells, we next sought to evaluate the effect of inhibiting Bax on the development of sarcopenia. First, we confirmed that treatment with the Bax inhibitor BAI1 in AGE-BSA-treated cells dose-dependently

suppressed the expression of Apaf1 and the activation of Casp3, Casp7, and Casp9 (Fig. S12).

We then assessed the impact of BAI1 on the progression of sarcopenia in HAGE-fed mice. Mice were randomly divided into three groups: one group was fed a LAGE diet, the second group was fed a HAGE diet, and the third group was fed a HAGE diet along with weekly intraperitoneal injections of BAI1 (Fig. 7A). During the 24-week experiment, there were no significant differences in non-fasting blood glucose and HbA1c levels between the BAI1-treated and HAGE groups, although both were markedly higher compared to the LAGE group (Fig. 7B and C). Levels of free and protein-bound CML and CEL, as well as elevated free MG-H1 in serum and skeletal muscle tissues, were significantly increased in both the BAI1-treated and HAGE groups compared to the LAGE group (Fig. 7D and I and S13). However, there was no significant difference in protein-bound MG-H1 between the BAI1-treated and LAGE groups (Fig. 7I and S13). These results suggested that BAI1 treatment did not influence the accumulation of AGEs in the serum and muscle tissues of mice.

Remarkably, BAI1 treatment partially inhibited the development of sarcopenia in HAGE-fed mice. Specifically, BAI1 partially improved grip strength (LAGE:  $79.1 \pm 8.4$  gm  $\times$  Force, HAGE:  $45.8 \pm 5.2$  gm  $\times$  Force, BAI1:  $62.3 \pm 7.1$  gm  $\times$  Force) (Fig. 7J), latency to fall (LAGE:  $21.5 \pm 3.2$  s, HAGE:  $10.2 \pm 1.5$  s, BAI1:  $15.5 \pm 2.4$  s) (Fig. 7K), and skeletal muscle mass index (LAGE:  $1.15 \pm 0.17\%$ , HAGE:  $0.53 \pm 0.04\%$ , BAI1:  $0.87 \pm 0.09\%$ ) (Fig. 7L). Histological analysis of skeletal muscle tissues demonstrated that BAI1 treatment significantly increased muscle fiber size and decreased connective tissue accumulation compared to the HAGE group (Fig. 7M). Quantitative assessment of CSA of muscle fibers further confirmed a marked increase in the BAI1-treated group relative to the HAGE group, although the CSA remained lower than that observed in the LAGE group (Fig. 7N). These physiological and pathological findings indicated that BAI1 treatment partially prevented the development of sarcopenia in HAGE-fed mice.

## Discussion

High levels of AGEs are positively correlated with the onset of sarcopenia, although the underlying molecular mechanisms remain unclear [31–34]. In this study, we established a mouse model of sarcopenia induced by high AGEs and identified hundreds of DEPs in sarcopenic muscle tissues through proteomic analysis. Our research focused on how PRMT1 mediated the CRTC3/FOXO3a/Bax/Caspases signaling axis, leading to apoptosis and ultimately contributing to the development of sarcopenia. Our results demonstrated

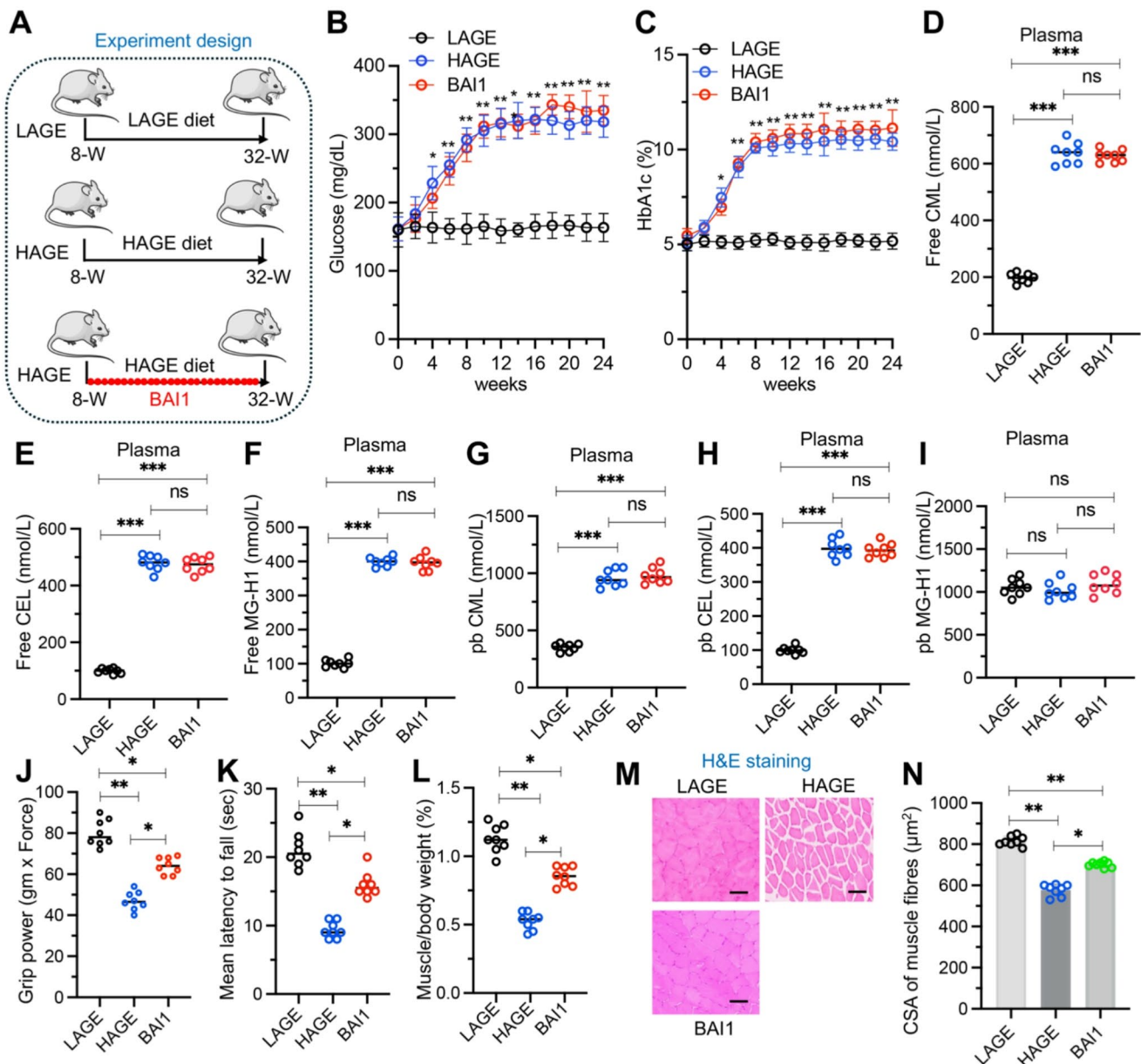


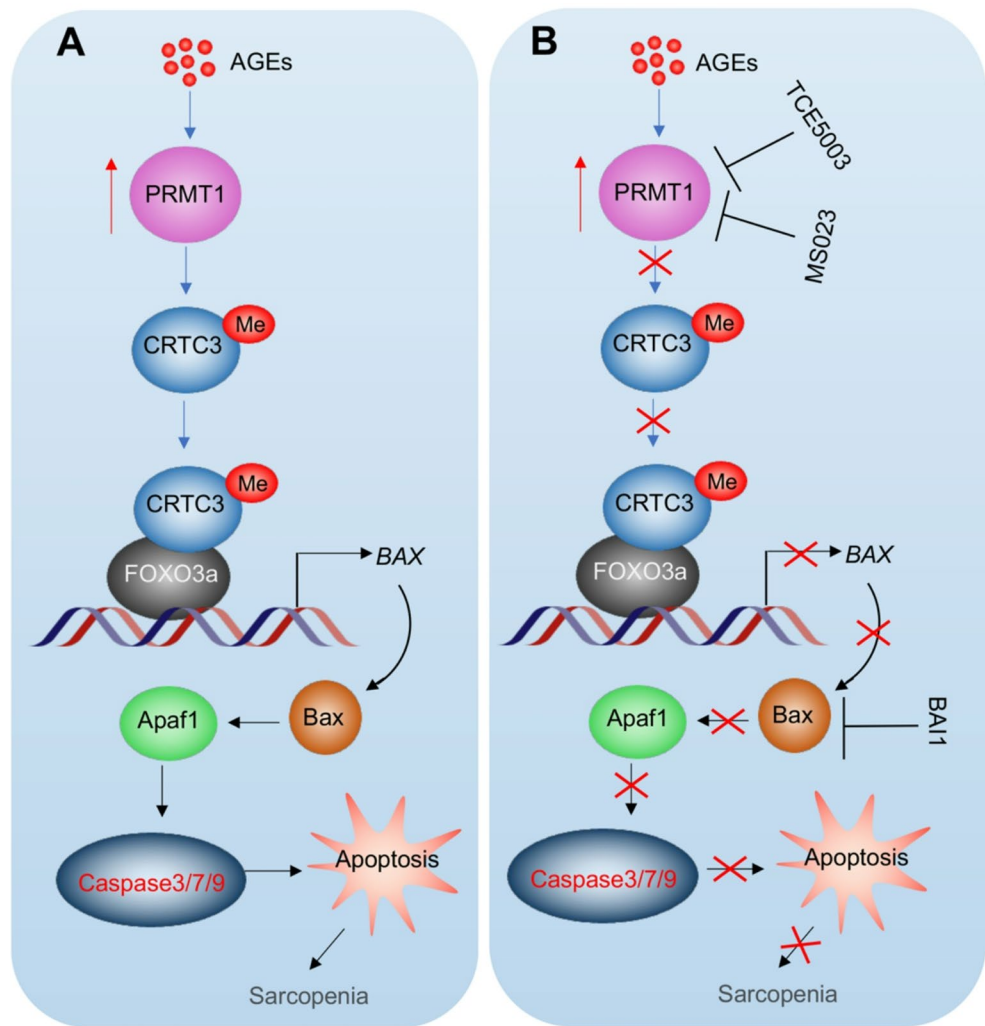
**Fig. 7** Administration of BAI1 partially prevented the development of sarcopenia in HAGE-fed mice. **(A)** Experimental design of BAI1 injection. **(B)** Non-fasting blood glucose levels in LAGE, HAGE, and HAGE+BAI1 groups of mice ( $n=8$  per group) at different time points. **(C)** HbA1c levels in LAGE, HAGE, and HAGE+BAI1 groups of mice ( $n=8$  per group) at different time points. **(D–I)** Concentrations of free and pb CML, CEL, and MG-H1 in plasma from LAGE, HAGE, and HAGE+BAI1 groups of mice ( $n=8$  per group). **(D)** Free CML

in plasma. **(E)** Free CEL in plasma. **(F)** Free MG-H1 in plasma. **(G)** pb-CML in plasma. **(H)** pb-CEL in plasma. **(I)** pb-MG-H1 in plasma. **(J)** Grip strength. **(K)** Latency to fall as assessed by the rotarod test. **(L)** Muscle-to-body weight ratio. **(M)** Representative images of skeletal muscle stained with H&E. Bars=100  $\mu\text{m}$ . **(N)** Quantified CSA of muscle fibers ( $\mu\text{m}^2$ ) ( $n=8$  per group). ns: no significant difference; \* $P<0.05$ ; \*\* $P<0.01$ ; \*\*\* $P<0.001$

that HAGE induced PRMT1, which modified the R534 site of CRTC3, leading to its activation and subsequent cooperation with FOXO3a to bind the *BAX* gene promoter, thereby upregulating *BAX* expression. The upregulation of Bax triggered downstream apoptotic signals, including the activation of Apaf1, Casp9, Casp3, and Casp7, resulting in intrinsic apoptosis (Fig. 8A). The application of the PRMT1

inhibitors (TCE5003 and MS023) and the Bax inhibitor BAI1 effectively blocked downstream Bax-mediated apoptotic signaling, inhibited apoptosis, and consequently partially prevented the progression of sarcopenia (Fig. 8B). Our findings elucidated a novel AGEs-dependent signaling pathway, expanded our understanding of PRMTs-mediated signaling in disease progression, and identified two potential

**Fig. 8** Schematic diagram of AGEs-mediated PRMT1/CRTC3/FOXO3a/Bax-dependent apoptotic signaling in the regulation of sarcopenia development. **(A)** Schematic representation of AGEs-mediated PRMT1/CRTC3/FOXO3a/Bax-dependent apoptotic signaling. Elevated levels of AGEs lead to the upregulation of PRMT1, which methylates the R534 site of CRTC3, resulting in its activation. The methylated CRTC3 then interacts with FOXO3a, forming a complex that binds to the BAX gene promoter and increases *BAX* expression. This upregulation of Bax initiates downstream apoptotic signaling pathways, including activation of Apaf1, Casp9, Casp3, and Casp7, culminating in intrinsic apoptosis. **(B)** Schematic representation of the effects of TCE5003, MS023, and BAI1 on sarcopenia progression. PRMT1 inhibitors (TCE5003 and MS023) and the Bax inhibitor (BAI1) collectively suppress Bax-mediated apoptotic signaling, reduce apoptosis, and mitigate the progression of sarcopenia



therapeutic targets that could offer new avenues for the clinical treatment of sarcopenia.

AGEs accumulate in various tissues and organs over time, particularly under conditions of hyperglycemia and oxidative stress [36, 37]. These AGEs are known to impact pathways that contribute to chronic inflammation, oxidative stress, and tissue remodeling, which are crucial factors in the progression of various diseases, including diabetes, cardiovascular diseases, neurodegenerative disorders, and chronic kidney disease [36, 37]. Recent studies have demonstrated that AGEs can promote intervertebral disc degeneration through the transactivation of *MMP* genes [30]. Mechanistically, HAGE activates p21-activated kinase 1 (PAK1), leading to the phosphorylation of peroxisome proliferator-activated receptor gamma coactivator-related protein 1 (PPRC1). Phosphorylated PPRC1, in conjunction with two histone acetyltransferases—p300/CREB-binding protein (CBP) and the transcription factor activator protein 1 (AP1)—enhances the expression of 12 *MMP* genes (*MMP 1a/1b/3/7/9/10/12/13/16/19/23/28*) [30]. In this study, we

demonstrated that elevated levels of AGEs upregulated PRMT1, which in turn catalyzed the methylation of CRTC3. Methylated CRTC3 interacted with FOXO3a, leading to the upregulation of the *BAX* gene and subsequent activation of Bax-mediated apoptotic signaling. Although our current research has elucidated a previously unrecognized AGE-regulated signaling pathway, two critical questions remain unanswered. Firstly, it is uncertain whether AGEs directly regulate PRMT1 expression as signaling molecules or if they influence PRMT1 indirectly by modifying the cellular microenvironment, such as through inflammatory or stress-related conditions. Secondly, it is not yet clear whether the effects of a HAGE diet on sarcopenia are reversible. To address these uncertainties, we plan to conduct future studies involving dietary modifications in mice. Specifically, we will design experiments where mice are initially fed a HAGE diet and subsequently switched to a LAGE diet, and alternatively, mice will start on a LAGE diet and then transition to a HAGE diet. These experimental models will allow us to evaluate physiological parameters, the expression of

apoptotic signaling molecules, and the progression of sarcopenia under varying dietary conditions. Such studies aim to provide a deeper understanding of the mechanisms through which a HAGE diet contributes to sarcopenia and to generate valuable data that could guide the development of potential therapeutic strategies for this condition.

In sarcopenia, the intrinsic (mitochondria-mediated) apoptotic pathway is often triggered by various cellular stressors, including oxidative stress and mitochondrial dysfunction [21–24]. The initiation of this pathway involves the disruption of mitochondrial integrity, leading to the release of pro-apoptotic factors like cytochrome c into the cytosol [21–24]. Cytochrome c then binds to apoptotic protease-activating factor 1 (Apaf-1), forming the apoptosome, which subsequently activates Casp9 [19, 20]. Once activated, Casp9 initiates a cascade of downstream effector caspases, such as Casp3 and Casp7, which execute the apoptotic process by degrading essential cellular components [19, 20]. The increased susceptibility of muscle cells to apoptosis in sarcopenia is driven by the upregulation of pro-apoptotic proteins like Bax and the downregulation of anti-apoptotic proteins such as Bcl-2, leading to a progressive loss of muscle fibers and a decline in muscle mass and strength [21–24]. Chronic inflammation and elevated oxidative stress associated with aging further exacerbate the activation of the intrinsic apoptotic pathway, accelerating muscle degradation [21–24]. While the overexpression of Bax has been documented in previous studies, the precise mechanisms underlying this phenomenon remain unclear. In our current study, we have identified that methylated CRTC3 and FOXO3a work in concert to transactivate the *BAX* gene. Furthermore, we have elucidated the upstream signaling involving PRMT1, demonstrating that the methylation of CRTC3 at the R534 site by PRMT1 is critical for its function. This newly uncovered signaling pathway not only deepens our understanding of Bax overexpression in sarcopenia but also provides insight into the mechanisms behind *BAX* gene overexpression in other types of diseases.

In this study, we observed an intriguing phenomenon: in AGE-BSA-treated cells and muscle tissues of HAGE-fed mice, several additional protein bands appeared above the normal CRTC3 band following its methylation modification. Interestingly, these bands were absent in the *in vitro* methylation assays performed with purified His-CRTC3 and also disappeared following treatment with TCE5003 or MS023, which coincided with the loss of CRTC3 methylation. This indicated that these bands were dependent on PRMT1-mediated methylation in a cellular context. However, the nature of these additional bands remains unknown. Since arginine methylation typically does not cause a significant shift in protein molecular weight, we hypothesize that CRTC3 undergoes additional post-translational

modifications following methylation, leading to altered electrophoretic mobility and the appearance of distinct protein bands. In future studies, we plan to utilize mass spectrometry to analyze these bands and elucidate the underlying mechanisms.

PRMT1-mediated arginine methylation plays a crucial role in regulating protein stability by modulating protein–RNA and protein–protein interactions [38–40]. This post-translational modification can alter the conformation and interaction dynamics of target proteins, thereby influencing their functional state and degradation rates [38–40]. For instance, PRMT1-mediated methylation of MLL2 (Mixed lineage leukemia 2) stabilizes the protein by preventing its poly-ubiquitylation, which would otherwise signal for its proteasomal degradation [39]. Similarly, PRMT1 enhances the stability of the transcription factor C/EBP $\beta$  (CCAAT/enhancer binding protein beta) by reducing the levels of the E3 ubiquitin ligase Smurf2 (SMAD-specific E3 ubiquitin-protein ligase 2), thereby diminishing C/EBP $\beta$  ubiquitination and degradation and ultimately facilitating adipogenesis [40]. In the present study, we found that HAGE promoted the accumulation of CRTC3 in a PRMT1-dependent manner. Although the precise mechanism by which this accumulation enhanced CRTC3 stability remained unclear, we hypothesize two potential mechanisms. First, arginine methylation may directly prevent the proteasomal degradation of CRTC3. Second, it may modulate protein–protein interactions that further stabilize CRTC3. In future research, we plan to investigate the stability, ubiquitination, and interacting partners of CRTC3 in PRMT1 knockdown cell lines treated with AGE-BSA, aiming to elucidate the regulatory mechanism by which methylation enhances CRTC3 stability.

We observed significant overlap among the top DEPs in skeletal muscle from HAGE-fed mice and C2C12 cells overexpressing PRMT1. This overlap strongly suggested that PRMT1 was a key effector molecule responding to AGEs. These findings highlighted PRMT1's role in amplifying AGE-induced molecular responses, which contributed to skeletal muscle atrophy. Furthermore, this overlap underscored the therapeutic potential of targeting PRMT1 to mitigate AGE-related pathologies, particularly in skeletal muscle. Such insights enhanced our understanding of PRMT1's involvement in AGE-induced muscle dysfunction and provided a foundation for developing novel therapeutic strategies. Moreover, our proteomic analysis of muscle tissues from HAGE-fed mice revealed not only the differential expression of PRMT1, CRTC3, and apoptosis-related molecules but also a significant upregulation of FTO, MMPs, and ADAMTSs. FTO, an RNA demethylase, is involved in regulating the expression of numerous key genes; however, its role in sarcopenia has not been previously reported.

MMPs and ADAMTSs are critical enzymes in the degradation of the extracellular matrix (ECM), a process essential to the development of sarcopenia. Therefore, these molecules likely play crucial roles in HAGE-induced sarcopenia. A particularly important finding in our study was that inhibition of PRMT1 and Bax only partially suppressed HAGE-induced sarcopenia. This partial suppression might be due to the involvement of MMPs, ADAMTSs, and other DEPs in the sarcopenia process, which meant that targeting PRMT1 and Bax alone was insufficient to fully inhibit the progression of the disease. In future studies, we will elucidate the mechanisms by which FTO, MMPs, and ADAMTSs contribute to sarcopenia and to explore additional targets for the prevention and treatment of this condition.

## Conclusions

Our study uncovered key molecular mechanisms by which AGEs contributed to sarcopenia. We identified a novel PRMT1-mediated CRTC3/FOXO3a/Bax/Caspases signaling pathway that drove apoptosis and muscle degradation in a mouse model of HAGE-induced sarcopenia. Inhibiting PRMT1 and Bax effectively slowed sarcopenia progression, underscoring their therapeutic potential.

**Supplementary Information** The online version contains supplementary material available at <https://doi.org/10.1007/s00018-025-05657-1>.

**Author contributions** Tian-Jin Huang: Methodology, Software, Data curation, Investigation. Shu Shang, Qin Wan, Qiang Li, Yang-Jingsi Li, and Jin-Na Zheng: Investigation, Software, Resources. Wentao Zhang: Investigation, Validation. Fa-Xiu Chen: Conceptualization, Resources, Writing - original draft, Writing - review & editing.

**Funding** This study was supported by the Natural Science Foundation of Jiangxi Province (Grant No. 20242BAB25539) and the Jiangxi Provincial Health Commission (Grant No. 202310009).

**Data availability** All data in this study are available from the corresponding author upon reasonable request.

## Declarations

**Ethical approval** All animal experiments were performed following a protocol (JPH-21-0012) approved by the Institutional Animal Care and Use Committee at Jiangxi Provincial People's Hospital.

**Consent for publication** All authors agree with the publication of this article.

**Competing interests** The authors declare that they have no known competing financial interests or personal relationships that could have appeared to influence the work reported in this paper.

**Open Access** This article is licensed under a Creative Commons Attribution-NonCommercial-NoDerivatives 4.0 International License, which permits any non-commercial use, sharing, distribution and reproduction in any medium or format, as long as you give appropriate credit to the original author(s) and the source, provide a link to the Creative Commons licence, and indicate if you modified the licensed material. You do not have permission under this licence to share adapted material derived from this article or parts of it. The images or other third party material in this article are included in the article's Creative Commons licence, unless indicated otherwise in a credit line to the material. If material is not included in the article's Creative Commons licence and your intended use is not permitted by statutory regulation or exceeds the permitted use, you will need to obtain permission directly from the copyright holder. To view a copy of this licence, visit <http://creativecommons.org/licenses/by-nc-nd/4.0/>.

## References

1. Papadopoulou SK (2020) Sarcopenia: A contemporary health problem among older adult populations. *Nutrients* 12:1293
2. Wiedmer P, Jung T, Castro JP, Pomatto LCD, Sun PY, Davies KJA et al (2021) Sarcopenia—Molecular mechanisms and open questions. *Ageing Res Rev* 65:101200
3. Jang YJ (2023) The effects of protein and supplements on sarcopenia in human clinical studies: how older adults should consume protein and supplements. *J Microbiol Biotechnol* 33:143–150
4. Gkekas NK, Anagnostis P, Paraschou V, Stamiris D, Dellis S, Kenanidis E et al (2021) The effect of vitamin D plus protein supplementation on sarcopenia: A systematic review and meta-analysis of randomized controlled trials. *Maturitas* 145:56–63
5. Cochet C, Belloni G, Buondonno I, Chiara F, D'Amelio P (2023) The role of nutrition in the treatment of sarcopenia in old patients: from restoration of mitochondrial activity to improvement of muscle performance, a systematic review. *Nutrients* 15:3703
6. Jang JY, Kim D, Kim ND (2023) Pathogenesis, intervention, and current status of drug development for sarcopenia: A review. *Bio-medicines* 11:1635
7. Najm A, Niculescu AG, Grumezescu AM, Beuran M (2024) Emerging therapeutic strategies in sarcopenia: an updated review on pathogenesis and treatment advances. *Int J Mol Sci* 25:4300
8. Rolland Y, Dray C, Vellas B, Barreto PS (2023) Current and investigational medications for the treatment of sarcopenia. *Metabolism* 149:155597
9. Twarda-Clapa A, Olczak A, Bialkowska AM, Koziolkiewicz M (2022) Advanced glycation end-products (AGEs): formation, chemistry, classification, receptors, and diseases related to ages. *Cells* 11:1312
10. Prasad C, Davis KE, Imrhan V, Juma S, Vijayagopal P (2019) Advanced glycation end-products and risks for chronic diseases: intervening through lifestyle modification. *Am J Lifestyle Med* 13:384–404
11. Uceda AB, Marino L, Casasnovas R, Adrover M (2024) An overview on glycation: molecular mechanisms, impact on proteins, pathogenesis, and Inhibition. *Biophys Rev* 16:189–218
12. Hwang JW, Cho Y, Bae GU, Kim SN, Kim YK (2021) Protein arginine methyltransferases: promising targets for cancer therapy. *Exp Mol Med* 53:788–808
13. Bedford MT, Richard S (2005) Arginine methylation an emerging regulator of protein function. *Mol Cell* 18:263–272
14. Blanc RS, Richard S (2017) Arginine methylation: the coming of age. *Mol Cell* 65:8–24
15. Liang W, Xu F, Li L, Peng C, Sun H, Qiu J et al (2024) Epigenetic control of skeletal muscle atrophy. *Cell Mol Biol Lett* 29:99

16. Choi S, Jeong HJ, Kim H, Choi D, Cho SC, Seong JK et al (2019) Skeletal muscle-specific Prmt1 deletion causes muscle atrophy via deregulation of the PRMT6-FOXO3 axis. *Autophagy* 15:1069–1081
17. Jeong HJ, Lee HJ, Vuong TA, Choi KS, Choi D, Koo SH et al (2016) Prmt7 deficiency causes reduced skeletal muscle oxidative metabolism and Age-Related obesity. *Diabetes* 65:1868–1882
18. Shin HJ, Kim H, Oh S, Lee JG, Kee M, Ko HJ et al (2016) AMPK-SKP2-CARM1 signalling cascade in transcriptional regulation of autophagy. *Nature* 534:553–557
19. Elmore S (2007) Apoptosis: A review of programmed cell death. *Toxicol Pathol* 35:495–516
20. Green DR, Llamas F (2015) Cell death signaling. *Cold Spring Harb Perspect Biol* 7:a006080
21. Marzetti E, Leeuwenburgh C (2006) Skeletal muscle apoptosis, sarcopenia and frailty at old age. *Exp Gerontol* 41:1234–1238
22. Marzetti E, Calvani R, Bernabei R, Leeuwenburgh C (2012) Apoptosis in skeletal myocytes: A potential target for interventions against sarcopenia and physical frailty—A mini-review. *Gerontology* 58:99–106
23. Cheema N, Herbst A, McKenzie D, Aiken JM (2015) Apoptosis and necrosis mediate skeletal muscle fiber loss in age-induced mitochondrial enzymatic abnormalities. *Aging Cell* 14:1085–1093
24. Wang H, Lustrat A, Meunier B, Gueugneau M, Coudy-Gandilhon C, Combaret L et al (2014) Apoptosis in capillary endothelial cells in ageing skeletal muscle. *Aging Cell* 13:254–262
25. Goodwin M, Herath C, Jia Z, Leung C, Coughlan MT, Forbes J et al (2013) Advanced glycation end-products augment experimental hepatic fibrosis. *J Gastroenterol Hepatol* 28:369–376
26. Liang YC, Cheng KP, Kuo HY, Wang CT, Chou HW, Huang KL et al (2023) Calsarcin-2 May play a compensatory role in the development of obese sarcopenia. *Biomedicines* 11:2708
27. Pacifici F, Della-Morte D, Piermarini F, Arriga R, Scioli MG, Capuani B et al (2020) Prdx6 plays a main role in the crosstalk between aging and metabolic sarcopenia. *Antioxid (Basel)* 9:329
28. Shang GK, Han L, Wang ZH, Liu YP, Yan SB, Sai WW et al (2020) Sarcopenia is attenuated by TRB3 knockout in aging mice via the alleviation of atrophy and fibrosis of skeletal muscles. *J Cachexia Sarcopenia Muscle* 11:1104–1120
29. Liu H, Lyu H, Jiang G, Chen D, Ruan S, Liu S et al (2022) ALKBH5-Mediated m6A demethylation of GLUT4 mRNA promotes Glycolysis and resistance to HER2-Targeted therapy in breast cancer. *Cancer Res* 82:3974–3986
30. Tseng C, Chen B, Han Y, Wang K, Song Q, Shen H et al (2024) Advanced glycation end-products promote intervertebral disc degeneration by transactivation of matrix metalloproteinase genes. *Osteoarthritis Cartilage* 32:187–199
31. Granic A, Hurst C, Dismore L, Dodds RM, Witham MD, Robinson SM et al (2023) Advanced glycation end-products in skeletal muscle health and sarcopenia: A systematic review of observational studies. *Mech Ageing Dev* 209:111744
32. Molinari P, Caldiroli L, Dozio E, Rigolini R, Giubbilini P, Corsi Romanelli MM et al (2022) Association between advanced glycation end-products and sarcopenia in patients with chronic kidney disease. *Biomedicines* 10:1489
33. Zhang X, Chen X, Li S, Gao M, Han P, Cao L et al (2024) Association between advanced glycation end-products and sarcopenia: the mediating role of osteoporosis. *J Clin Endocrinol Metab* 109:e1105–e116
34. Eguchi Y, Toyoguchi T, Inage K, Fujimoto K, Orita S, Suzuki M et al (2021) Advanced glycation end-products are associated with sarcopenia in older women: aging marker dynamics. *J Women Aging* 33:328–340
35. Ostojic J, Yoon YS, Sonntag T, Nguyen B, Vaughan JM, Shokhiev M et al (2021) Transcriptional co-activator regulates melanocyte differentiation and oncogenesis by integrating cAMP and MAPK/ERK pathways. *Cell Rep* 35:109136
36. Takeuchi M, Sakasai-Sakai A, Takata T, Takino JI, Koriyama Y (2022) Effects of toxic ages (TAGE) on human health. *Cells* 11:2178
37. Zhou M, Zhang Y, Shi L, Li L, Zhang D, Gong Z et al (2024) Activation and modulation of the AGEs-RAGE axis: implications for inflammatory pathologies and therapeutic interventions—A review. *Pharmacol Res* 206:107282
38. Guccione E, Richard S (2019) The regulation, functions and clinical relevance of arginine methylation. *Nat Rev Mol Cell Biol* 20:642–657
39. An D, Kim J, Moon B, Kim H, Nguyen H, Park S et al (2024) PRMT1-mediated methylation regulates MLL2 stability and gene expression. *Nucleic Acids Res* gkae1227
40. Zhu Q, Wang D, Liang F, Tong X, Liang Z, Wang X et al (2022) Protein arginine methyltransferase PRMT1 promotes adipogenesis by modulating transcription factors C/EBP $\beta$  and PPAR $\gamma$ . *J Biol Chem* 298:102309

**Publisher's note** Springer Nature remains neutral with regard to jurisdictional claims in published maps and institutional affiliations.